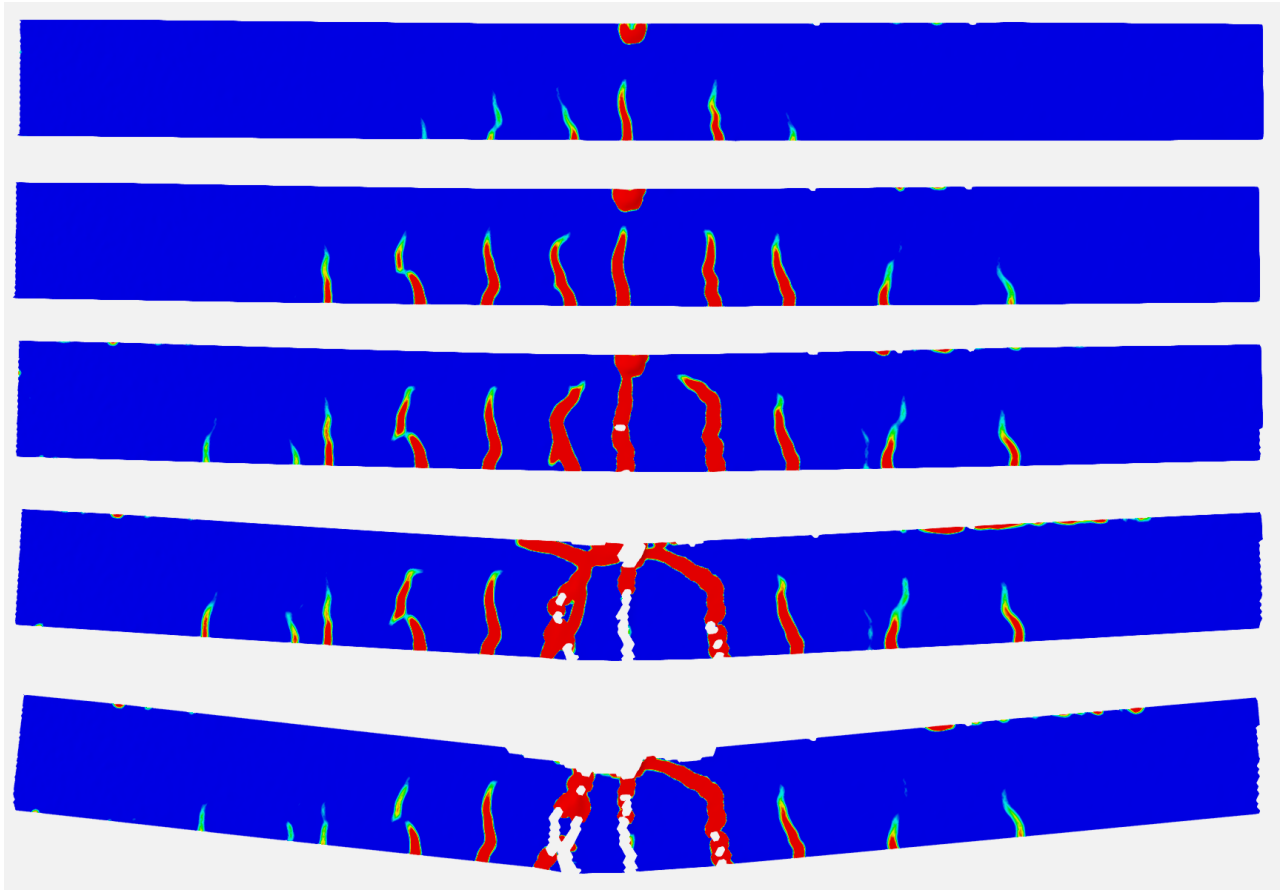




CHALMERS
UNIVERSITY OF TECHNOLOGY



Evaluation of crack width predictions in Eurocode 2 using Digital Image Correlation

Master's Thesis in Structural Engineering and Building Technology

PRZEMYSŁAW SMEREKA

Department of Architecture and Civil Engineering
Division of Structural Engineering
Concrete Structures
CHALMERS UNIVERSITY OF TECHNOLOGY
Master's Thesis ACEX30-19-105
Gothenburg, Sweden 2019

MASTER'S THESIS ACEX30-19-105

Evaluation of crack width predictions in Eurocode 2 using Digital Image Correlation

Master's Thesis in the Master's Programme Structural Engineering and Building Technology

PRZEMYSŁAW SMEREKA

Department of Architecture and Civil Engineering

Division of Structural Engineering

Concrete Structures

CHALMERS UNIVERSITY OF TECHNOLOGY

Göteborg, Sweden 2019

Evaluation of crack width predictions in Eurocode 2 using Digital Image Correlation

Master's Thesis in the Master's Programme Structural Engineering and Building Technology

PRZEMYSLAW SMEREKA

© PRZEMYSLAW SMEREKA 2019

Examensarbete ACEx30-19-105

Institutionen för arkitektur och samhällsbyggnadsteknik

Chalmers tekniska högskola, 2019

Department of Architecture and Civil Engineering

Division of Structural Engineering

Concrete Structures

Chalmers University of Technology

SE-412 96 Göteborg

Sweden

Telephone: + 46 (0)31-772 1000

Cover:

Reinforced concrete beams, GOM Correlate Professional, Digital Image Correlation

Department of Architecture and Civil Engineering

Göteborg, Sweden, 2019

Evaluation of crack width predictions in Eurocode 2 using Digital Image Correlation
Master's thesis in the Master's Programme Structural Engineering and Building Technology

PRZEMYSŁAW SMEREKA

Department of Architecture and Civil Engineering
Division of Structural Engineering
Concrete Structures
Chalmers University of Technology

ABSTRACT

A correct prediction of crack widths in reinforced concrete elements in Serviceability Limit State (SLS) is important in terms of keeping the proper functionality of the structure. The purpose of this thesis was to investigate the accuracy of crack width predictions using Eurocode 2 (EC 2) and ACI 224R compared with three-point bending tests on simply supported reinforced concrete beams.

The crack widths were measured using normal speed cameras recording at a rate of 0.5 frames per second (fps). Later on, the data was processed using Digital Image Correlation (DIC). A strain field of the studied beam has been created using the 3D software GOM Correlate Professional. The crack widths were measured by creating two facet points per each crack directly at the level of bottom reinforcement. Horizontal displacements between these points were calculated giving a precise value of crack widths which appeared in the cracked cross-sections of reinforced concrete beams. Corresponding reinforcement stresses in cracked cross-sections were calculated and plotted in a stress-crack width relation, together with the theoretical values coming from EC 2 and ACI 224R.

The direct location of the cracks was measured using two different reference points using DIC. The accuracy for the measured crack spacing was estimated to ± 5 mm and for crack widths estimated to ± 0.01 mm. As expected, the largest cracks appeared in the middle section of the beam where the cross-sectional stresses are the highest.

The results show that the maximum crack spacing and the mean value of crack spacing is accurately predicted by EC 2. Furthermore, EC 2 gives a quite good estimation for the mean values of crack widths whereas ACI 224R seems to overestimate the mean crack widths. When comparing the maximum crack widths, it can be observed that EC 2 gives a very precise prediction which corresponds with DIC results. However, in some of the cases especially in the beginning stage of crack propagation it can be noted that both EC 2 and ACI 224R overestimates the crack widths.

Key words: Digital Image Correlation, DIC, reinforced concrete, simply supported beams, static loading, Eurocode 2, ACI 224R, GOM Correlate Professional, crack widths, crack spacing, Serviceability Limit State, SLS

Contents

ABSTRACT	I
CONTENTS	II
PREFACE	V
NOTATIONS	VI
1 INTRODUCTION	1
1.1 Background	1
1.2 Aim and objectives	2
1.3 Methods	2
1.4 Limitations	2
2 REVIEW OF BACKGROUND THEORY	3
2.1 Material behaviour	3
2.1.1 Concrete	3
2.1.2 Reinforcement	5
2.1.3 Work states during bending in reinforced concrete beams	7
2.2 Constitutive models	8
2.2.1 Modelling of crack response	8
2.2.2 Interaction between reinforcement and concrete	11
2.3 Crack width predictions	12
2.3.1 Crack widths according to Eurocode 2	12
2.3.2 Crack widths according to ACI	14
2.4 Multi-level Assessment Strategy	14
2.5 Finite element analysis	15
2.6 Previous research	18
3 EXPERIMENT DESCRIPTION	20
3.1 Beam geometry and material properties	20
3.1.1 Concrete properties	21
3.1.2 Steel properties	22
3.2 Static tests procedure	23
3.2.1 Three-point bending tests	23
3.3 Digital Image Correlation	25
4 COMPARISON OF RESULTS	26
4.1 General	26
4.2 Crack spacing	30
4.3 Crack widths	32

5	CONCLUSIONS	38
5.1	General conclusions	38
5.2	Future studies	38
6	REFERENCES	40
APPENDIX A CALCULATIONS		41
A.1	Input data	41
A.1.1	Geometry and static scheme of the beam	41
A.1.2	Concrete properties	42
A.1.3	Reinforcement properties	42
A.2	Load capacity excluding top reinforcement	43
A.3	Load capacity including top reinforcement	44
A.4	Load capacity summary	44
A.5	Crack widths calculations	45
A.5.1	Loads	45
A.5.2	Crack widths according to Eurocode 2	45
A.5.3	Crack widths according to ACI 224R	46
A.5.4	Crack widths summary	47

Preface

The possibility to accurately evaluate crack widths using Eurocode 2 and ACI 224R guidelines was studied in this master thesis. The data was processed using GOM Correlate Professional based on three-point bending experiments on reinforced concrete beams which were performed in Chalmers in 2017 and compared with common crack width calculation methods.

A lot of individuals supported me in development of this master thesis. First of all, I would like to express my deepest gratitude to my main supervisor, Associate Professor Mario Plos for his support throughout the whole process of creating this master thesis. I greatly appreciate the time and effort he took to explain things to me, down to a level where I could really understand the problem. Without his help from the very beginning of when I arrived to Chalmers, this master thesis would not be completed. I am also very grateful for the support I received from my second supervisor Adjunct Professor Morgan Johansson, who shared his deep knowledge with me during the process of writing this master thesis. I would like to especially thank him for his help in breaking down complex problems in a simple way, which was easy to understand and implement into the project.

Furthermore, I would like to thank Senior Lecturer Joosef Leppänen for his encouragement throughout the process of writing this master thesis and for providing the essential tools for this project. Additionally, I truly appreciate the support from Mathias Flansbjerg, for sharing his knowledge about Digital Image Correlation and practical advices during processing the data in GOM Correlate Professional. I also thank my opponent Julius Kandt for giving great comments to my final report.

Sincere thanks to all my friends for the unlimited support which I received during the whole period of my studies. Finally, I would like to thank my family, especially my parents and grandparents for always believing in me and always supporting me with my decisions. Without you, I would never be in the place where I am right now.

Göteborg, June 2019

Przemyslaw Smereka

Notations

Latin upper case letters

A	Cross-section area of reinforcing bar
A_{s1}	Cross-sectional area of tension reinforcement
A_{s2}	Cross-sectional area of compressive reinforcement
E	Modulus of elasticity
E_{cm}	Modulus of elasticity of concrete
E_s	Modulus of elasticity of steel
G_f	Fracture energy
I_I, I_{II}	Moment of inertia in state I and state II respectively
L	Beam length
L_i	Beam span
M	Bending moment in a studied cross-section
M_{cr}	Cracking moment
M_{Rd}	Load capacity of a bended cross-section
W_c	Section modulus

Latin lower case letters

a_2	Top reinforcement centre of gravity
b	Cross-section width
c	Neutral axis depth
c_c	Concrete cover
d	Effective depths of the cross-section
f_{cd}	Design value of concrete compressive strength
f_{cm}	Mean value of concrete cylinder compressive strength
$f_{cm,cube}$	Mean value of concrete cube compressive strength
f_{ct}	Axial tensile strength of the specimen
f_{ctm}	Mean value of axial tensile strength of concrete
$f_{ct,sp}$	Splitting tensile strength of the specimen
f_r	Modulus of rupture of concrete
f_s	Stress in tension reinforcement in a cracked section according to ACI 224R
f_u	Ultimate steel stress
f_y	Mean yield strength
f_{yd}	Design value of yield strength of reinforcement
$f_{0.2}$	Proof steel stress
h	Cross-section height
h_b	Crack band width
k_1	Coefficient which takes into account the bond properties of reinforcement
k_2	Coefficient which takes into account the distribution of strains
k_t	Factor dependent on the duration of load
l_{elem}	Length of the FE element
s	Bar spacing
s_m	Mean crack spacing
s_{p1}	Slip corresponding to bond strength
$s_{r,max}$	Maximum crack spacing
s_{rm}	Mean crack distance

w	Maximum crack width according to ACI 224R
w_d	Deformation of one crack
w_k	Characteristic crack width according to EC2
w_m	Characteristic crack width according to EC2
x_I, x_{II}	Height of the compressive zone in state I and state II respectively

Greek lower case letters

α	Powers in bond stress-slip relations
α_e	Ratio between steels and concrete modulus of elasticity
β	Ratio of distance between neutral and tension face to distance between neutral axis and centroid of reinforcing steel
γ	Reinforced concrete weight
γ_c	Partial factor for concrete
γ_s	Partial factor for steel
ε	Strain
ε_{cm}	Mean strain in concrete between cracks
ε_{cu}	Ultimate concrete strain
ε_{sm}	mean strain in reinforcement under relevant combination loads
ε_{su}	Ultimate steel strain
λ	Modification factor for lightweight concrete
ν	Poisson's ratio
ξ_{eff}	Relative height of the compressive zone
$\rho_{s,eff}$	Effective reinforcement ratio
σ	Stress
σ_c	Stress in concrete in a cracked section
σ_s	Stress in tension reinforcement in a cracked section according to EC2
τ_{max}	Bond strength
\emptyset	Reinforcing bar diameter

1 Introduction

1.1 Background

There are doubts regarding how precise simple formulas can predict crack widths due to a large number of factors that affect the appearance of the cracks. Maintaining sufficiently small crack widths in reinforced concrete elements in serviceability limit state (SLS) is crucial to ensure the proper functionality and appearance of the structure. If the cracks are too large, they can expose the reinforcement to environmental conditions, which can lead to corrosion and can affect the durability of the structure. In engineering practice, crack widths are determined using empirical models, and a distribution of sectional forces based on the classic and simple linear theory (assuming that both concrete and steel are fully linear materials) which could possibly lead to overestimation of the crack widths.

Nonlinear finite element (FE) analysis is a powerful tool to predict and better understand the structural response of a reinforced concrete structure. In previous research projects at Structural Engineering, Chalmers, it has been studied when to use different level of detailing in structural assessment of reinforced concrete slabs. The proposed strategy for multi-level structural assessment, (Plos et al., 2017) is based on the principle of successively improved evaluation in structural assessment. For increased levels of detailing the following structural analysis levels are proposed:

- (I) Simplified analysis
- (II) 3D linear FE analysis
- (III) 3D nonlinear shell FE analysis
- (IV) 3D nonlinear FE analysis with continuum elements and fully bonded reinforcement
- (V) 3D nonlinear FE analysis with continuum elements including the slip between reinforcement and concrete.

The more advanced method used, the better understanding of the structural response is obtained. However, the computation time and complexity of the calculations also increases. Previous work, though, has been mainly focused on the ultimate limit state (ULS), and therefore, there is a need to further study how to correctly predict the response including crack widths in SLS. As a basis of such study, accurate and statistically quantified crack width measurement from experiments are needed.

Crack propagation and material deformation during experiments can be very hard to track without proper tools. Digital Image Correlation (DIC) is a technique which works by comparing digital photographs of the tested specimens on different stages of deformation. By tracking blocks of pixels, the system can measure surface displacement and build full field 2D and 3D deformation and strain maps. This type of experimental data is very well suited for comparison and verification with Eurocode 2 calculations and possibly with non-linear FE analysis results.

1.2 Aim and objectives

The aim of this study was to investigate the possibility to accurately evaluate crack widths in reinforced concrete structures mostly based on Eurocode 2 guidelines, and to deepen the knowledge and understanding of how Digital Image Correlation can be used for verification of the calculated crack widths. The main objectives of this thesis are listed below:

- Investigate state-of-art regarding crack width evaluation based on Eurocode 2 standards
- Evaluate the crack widths in reinforced concrete beams using the software GOM Correlate Professional.
- Compare the obtained DIC results to common crack width calculation methods.
- Study statistical distribution of crack widths in reinforced concrete beams.
- Based on the results, suggest methods for crack width evaluation which give the most accurate and realistic results.
- Suggest methods which can further develop crack width evaluation in reinforced concrete elements in future studies.

1.3 Methods

At the start of the project a literature study was performed to deepen the knowledge on cracking behavior of concrete and response in SLS in general. In particular, the possibility to accurately predict crack widths using Eurocode 2 and DIC was studied. Additional literature studies concerning other methods of crack width evaluation were performed which could be relevant for further studies of the problem. The reinforced concrete beams were previously tested at Chalmers using three-point bending tests.

The results were acquired using an optical system called DIC. The obtained experimental DIC results were then compared with common crack width calculation methods by creating graphs related to stress in tensile reinforcement and crack widths in different stages of loading. The stresses were calculated in different sections of the beams which represented the exact positioning of the cracks. The crack positioning in particular beams were described using a simple schematic line graph showing the crack spacing and appearance of each particular crack in the beam. The graphs were followed up by images from GOM Correlate Professional in order to keep the crack positioning as clear as possible. Methods of the most accurate crack width evaluation were suggested, based on the results.

1.4 Limitations

The experiments were limited to one load setting using point loads but excluding long-term loading. The specimens which were used for experiments could have initial micro-cracks due to shrinkage of concrete and the changes of temperature between the specimen and surrounding area. The tested beams had the same cross-section 100x100 mm. To provide a full range of results, long term-loading and bigger cross-sections could be tested in the future.

2 Review of background theory

2.1 Material behaviour

2.1.1 Concrete

Concrete is a material which is widely used all over the world in construction because of its high compressive strength, durability and low ratio between costs and strength compared to other available materials. It's a composite material consisting of aggregate, cement matrix, contact zones and voids containing water or air. Therefore, the structure of concrete is strongly heterogeneous and the distribution of stresses during compression is uneven as illustrated in Figure 2.1 (Tejchman & Bobinski, 2014).

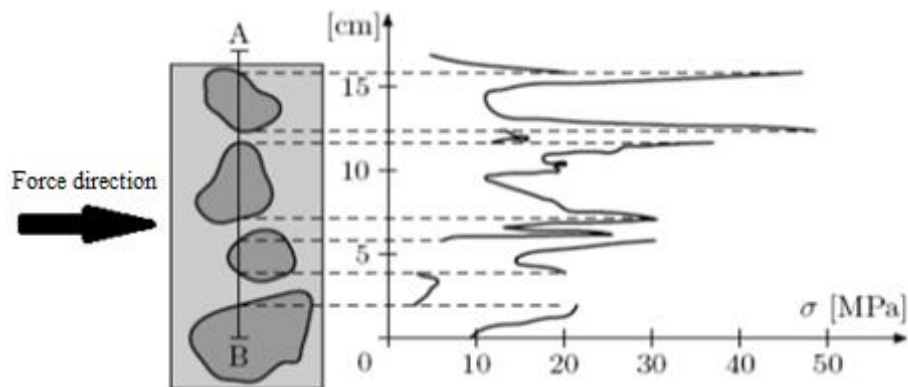


Figure 2.1 Distribution of stresses in concrete subjected to compression based on (Tejchman & Bobinski, 2014)

Both in compression and tension concrete is known for its nonlinear behaviour. Figure 2.2. presents a typical uniaxial stress-strain relationship. According to (Tejchman & Bobinski, 2014) when concrete is submitted to uniaxial compression the material approximately behaves elastically up to 30% of its compressive strength. After reaching this point the behaviour starts to be nonlinear. When specimen is submitted to compression loading the cracks are parallel to the loading direction. During uniaxial tension a linear behaviour can be observed up to 60% of its tensile strength (Tejchman & Bobinski, 2014). Cracking occurs here perpendicular to the loading direction. Consequently, to accurately estimate the response of a concrete structure it is essential to include the nonlinearity of the material during calculations.

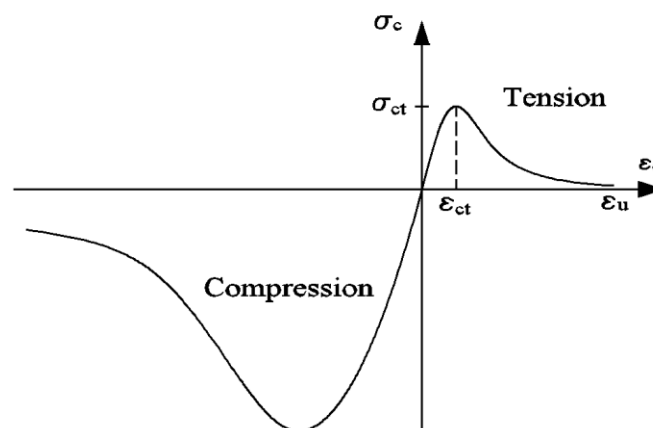


Figure 2.2 General appearance of material response in concrete

The failure of an unreinforced concrete specimen is governed by the micro-crack propagation. In reality, even before loading of the specimen there exist micro-cracks between the aggregates and the cement paste. They appear because of inevitable differences of properties between aggregate and cement paste. Other causes of this phenomenon are thermal stresses combined with concrete shrinkage after casting of concrete. During tensile loading of the specimen micro-cracks appear at local weak points in the material. When the load increases further, micro-cracks in the cement paste connect with micro-cracks coming from the lack of bond to the aggregates. In this way deformations begins to localize into a zone of micro-cracks at the weakest section of the specimen. When the maximum load is reached, the material outside this zone becomes unloaded and the deformations increase. The micro-cracks finally lead to separation of the material on each side of the fracture zone and no further stresses can be transferred across the cracks. (Plos, 2000)

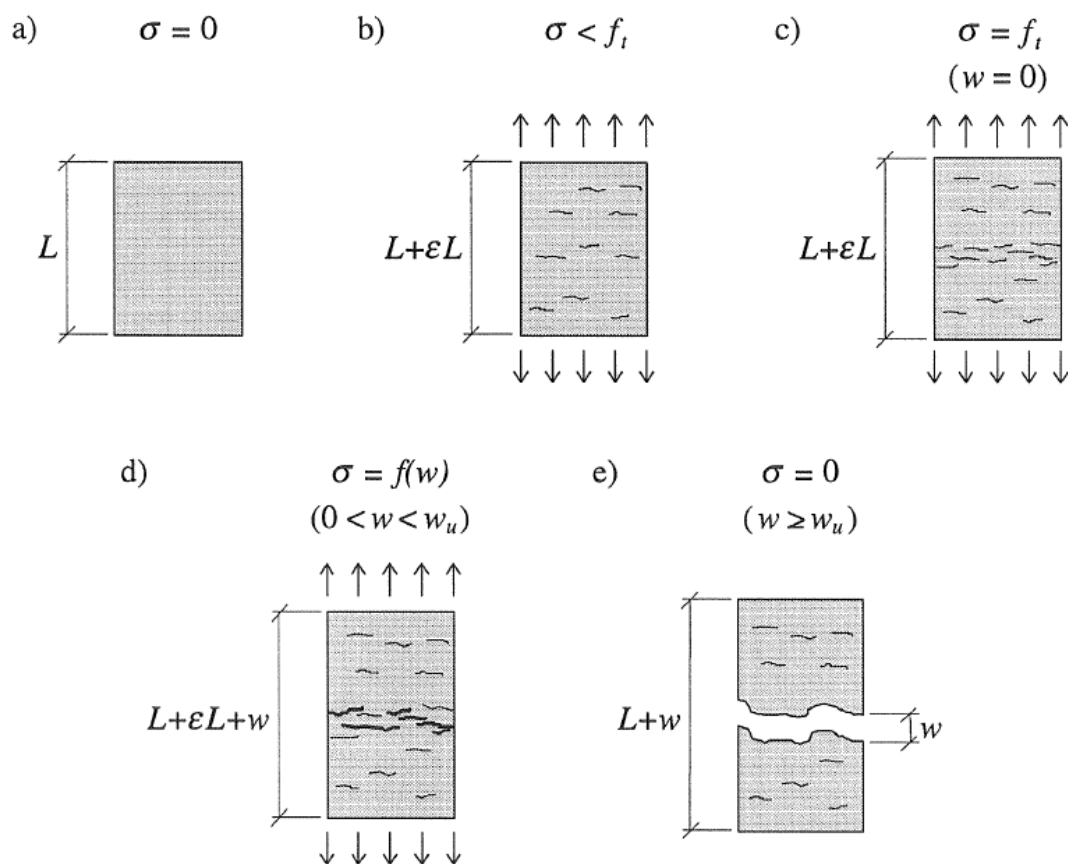


Figure 2.3 Fracture development in a concrete specimen, uniaxially loaded to failure with increasing deformation. (Plos, 2000).

It should be noted that considering energy of cracking, it is easier to further propagate an already existing crack than to create a new crack. This explains why the deformations in the specimen in Figure 2.3 localizes into one major crack, while the micro-cracks outside this crack becomes unloaded. To reflect this localisation, the concrete response is generally subdivided into a stress-strain relation and a stress-crack opening relation, as shown in Figure 2.4.

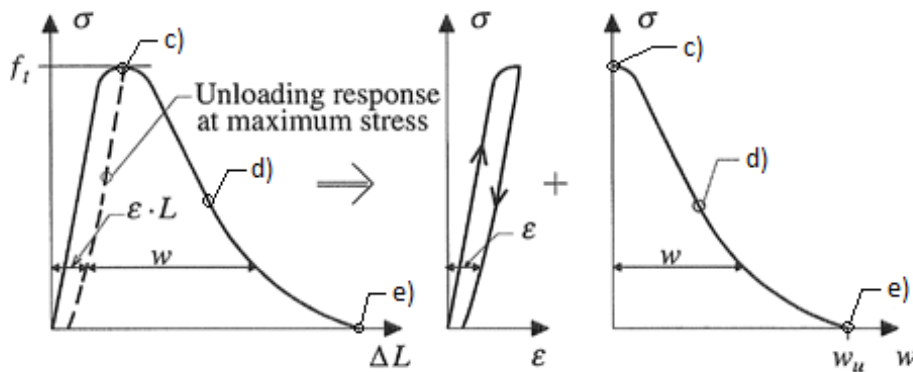


Figure 2.4 Mean stress-displacement relation for the uniaxial test specimen in Figure 2.3 based on (Plos, 2000), subdivided in a stress-strain response for the uncracked concrete and a stress-crack width response for the crack. The fracture development stages in Figure 2.3 (a-e) are indicated in the figure.

The response of concrete cracks is characterized by the tensile strength, shape of the stress-crack opening response and the fracture energy which is the energy needed to completely break a unit area of a material. In general, fracture energy can be calculated using relatively simple formulas using two parameters which are the tensile strength and the aggregate size. Additionally, during three-point bending tests a precise and stable shape of load-deflection curve can be obtained. Thus, the consumption of energy is represented by the area under the curve during crack propagation. Once the cross-section area is known then it is possible to rather easily calculate the fracture energy.

2.1.2 Reinforcement

The reinforcement interacts with concrete during loading mainly by carrying tensile stresses. In reinforced concrete structures reinforcement is usually placed within the areas where tensile forces are expected. Mechanical properties of reinforcement steel are dependent on the type of steel and its chemical composition. Stress-strain diagrams for different classes of common mild reinforcement steel during uniaxial tension are shown in Figure 2.5. It can be observed that the extension of the plastic region of the used reinforcement decreases with increasing tensile strength.

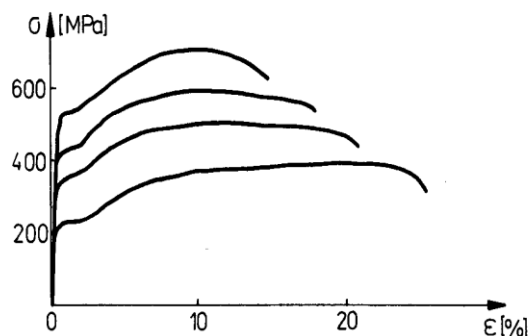


Figure 2.5 Stress-strain diagram for different types of mild steel during uniaxial tension (Tejchman & Bobinski, 2014)

Figure 2.6 shows that between points 0-1 Hooke's law is applicable – strains and stresses have a linear relation:

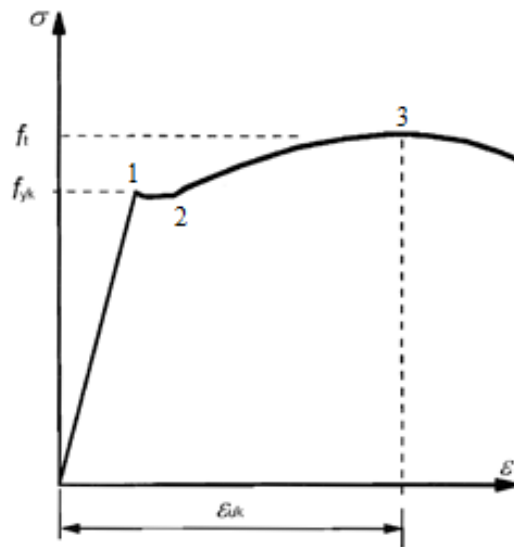


Figure 2.6 Stress-strain diagram of typical hot rolled steel reinforcing steel under uniaxial tension based on (Kobiak & Stachurski, 1984) and (EN 1992-1-1, 2004).

$$\sigma = E\varepsilon \quad (2.1)$$

$$\varepsilon = \frac{\Delta l}{l} \quad (2.2)$$

$$\sigma = \frac{F}{A} \quad (2.3)$$

Where:

σ	Stress
ε	Strain
l	Is the length of bar and Δl its elongation when subjected to the force F
E	Is the Young's modulus
A	The cross-sectional area of bar

From point 1 and further the diagram is not linear which means that Hooke's law is not applicable anymore. From point 1 to 2 steel elongates under constant stresses. This plastic response is very important in design of reinforced concrete elements. The value of stress in the plastic region is called the yield strength, f_{yk} . Further loading from point 2, until point 3, causes hardening of the steel with increased stresses and strains. In point 3 the specimen reaches the highest value of stresses f_t which is the tensile strength of steel (Kobiak & Stachurski, 1984).

2.1.3 Work states during bending in reinforced concrete beams

During bending we can distinguish three main work states of a reinforced concrete structure under increased loading.

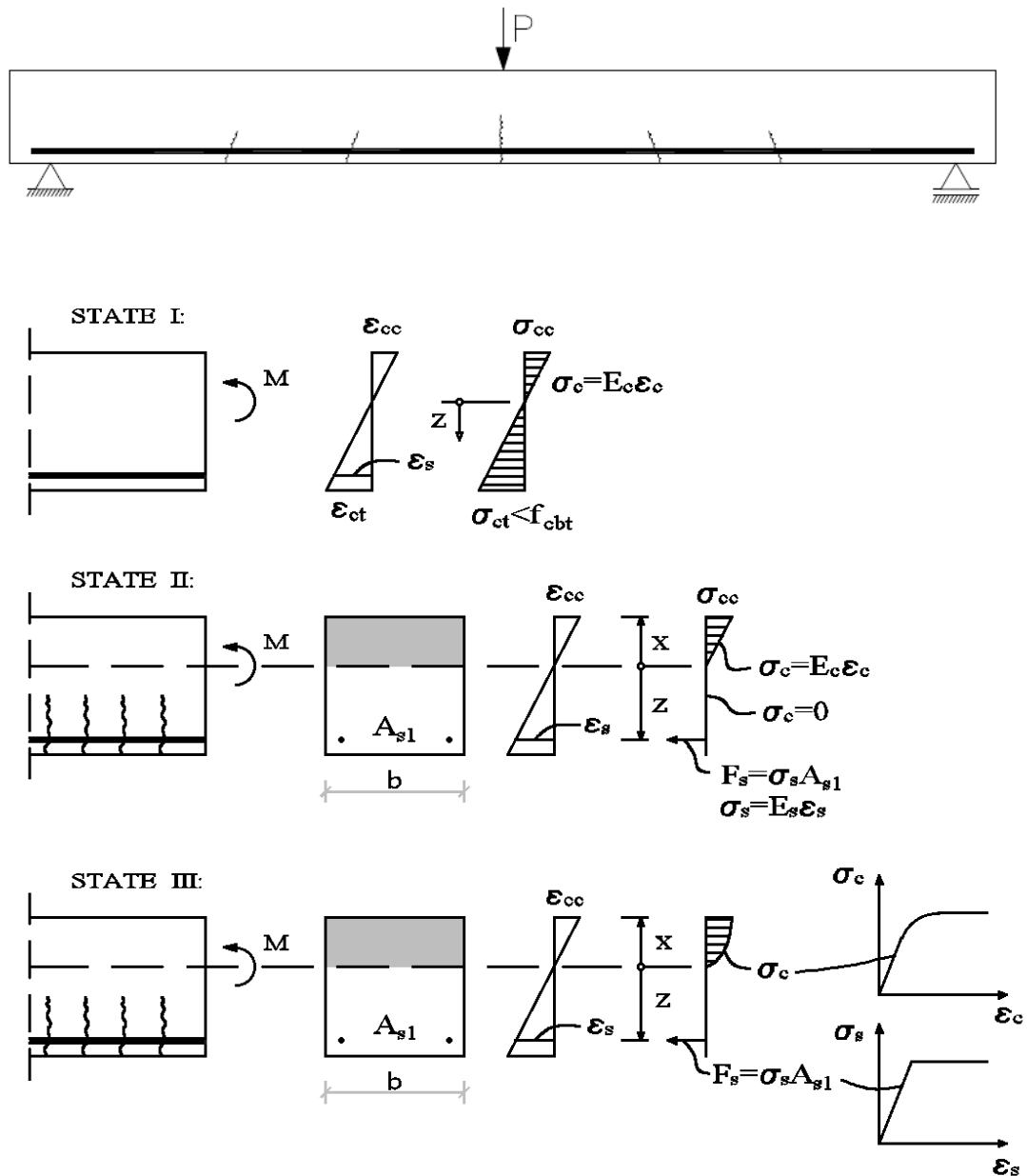


Figure 2.7 Different work states in reinforced concrete beam based on (Engström, 2011).

In state I stresses in concrete are so small that an assumption can be made that concrete and reinforcement are treated as a linear-elastic material (according to Hooke's Law) at this point the cross-section is still uncracked. The limit between state I and II is assumed as the cracking moment M_{cr} , reached when the largest concrete stresses equals the tensile strength f_{ctm} as in the formula presented in equation (2.4). In state II the stresses in the compressive zone are still elastic. An assumption is made that below the neutral axis, concrete does not carry stresses anymore. While analysing state III the stresses in concrete are becoming nonlinear. However, the stresses below the neutral axis are still carried by the reinforcement in a similar manner as in state II (Engström, 2011)

During bending:

$$M_{cr} = f_{ctm} \cdot W_c \quad (2.4)$$

Section modulus:

$$W_c = \frac{I_I}{h - x_I} \quad (2.5)$$

Where:

I_I	Moment of inertia in stage I (before cracking)
h	Cross-section height
x_I	Height of the compressive zone in stage I (before cracking)
f_{ctm}	Mean value of axial tensile strength of concrete

The cracked state II can be also divided into state IIa where compression stresses are still relatively small and a linear response for the uncracked concrete can be assumed and state IIb, where concrete is assumed to not carry any stresses below the neutral axis (the stresses are carried by the reinforcement). Stresses in concrete are so big that the compressive zone becomes plastic and the stress diagram is strongly nonlinear. In stage III the stress reaches its maximum value. It means that the limit state has been reached.

2.2 Constitutive models

2.2.1 Modelling of crack response

2.2.1.1 Crack initiation

The cracking process in concrete is complicated and the crack pattern can vary due to many factors. The conventional criterion for a homogenous structure assumes that when the principal tensile stresses reach the value of uniaxial strength of concrete then cracking in the structure will initiate (Cai, 2007). To study the nonlinearity caused by cracking in concrete it is important to know the crack initiation process. Various criteria were proposed by researchers to indicate the cracking initiation. In nonlinear analyses we generally deal with 2D or 3D stress state. For such cases a more general crack initiation criterion is needed taking into account the multidirectional stress state (in 3D often expressed as a part of the failure surface). Crack direction is generally assumed to be perpendicular to the maximum principal stress at crack initiation.

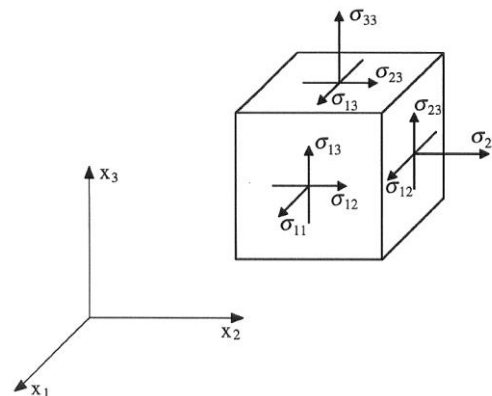


Figure 2.8 The stress state at a point, represented by stress components.

The values of the stress component will change while the cube (Figure 2.8) changes its position (coordinates) in its global coordinate system. When oriented in the principal directions the shear components σ_{12} , σ_{13} , σ_{23} will become zero. Since isotropic materials have the same properties in all directions, the material behaviour is often expressed in much more simplified ways. In particular by relations between principal stresses and principal strains. In plane stress analysis the matrix can be simplified as follows:

$$\begin{bmatrix} \sigma_x \\ \sigma_y \\ \sigma_{xy} \end{bmatrix} = \begin{bmatrix} \frac{E}{1-\nu^2} & \frac{\nu E}{1-\nu^2} & 0 \\ \frac{\nu E}{1-\nu^2} & \frac{E}{1-\nu^2} & 0 \\ 0 & 0 & \frac{E}{1-\nu^2} \end{bmatrix} \cdot \begin{bmatrix} \varepsilon_x \\ \varepsilon_y \\ \varepsilon_{xy} \end{bmatrix} \quad (2.6)$$

Where:

E Is the Young's modulus
 ν Is the Poisson's ratio

2.2.1.2 Discrete crack models

One way to model the crack response in an FE analysis is to model the discrete crack using separate elements. To represent the cracks, nonlinear spring elements can be introduced across the crack. An alternative is to use interface elements which can adequately express the track-displacement relation of the crack. The optimal situation is when we do not obtain deformations in the crack elements before the crack initiation. When it comes to the material between the cracks, usually continuum elements are used because they are able to take into account the nonlinear behaviour of the material in compression, for example using plasticity theory.

Advantages of discrete crack approach:

- The material response is used directly.
- Just like in the reality, crack is described as a discontinuity.

Disadvantages of discrete crack approach:

- Special interface elements are needed.
- Localisation of the crack needs to be known in advance which can be a problem while analysing more complex structures.

2.2.1.3 Smeared crack models

An alternative is to include the crack response in the response of the continuum elements using a smeared crack model. In smeared crack models crack discontinuity is smeared out over continuum elements. Consequently, the stress-strain response of the concrete in the continuum element must include the cracking behaviour. Initially, the material response can be described by an isotropic stress-strain relation. However, this state holds up only until the crack initiation. Once the crack criterion is satisfied, the stress-strain relation begins to be orthotropic. In this case we are able to obtain certain regions of distributed cracking. Therefore, using this model we cannot detect individual cracks. One of the most common crack initiation criteria which is being used in smeared crack models is the Rankine criterion – the crack initiates once the largest principal stress reaches the value of tensile strength (Plos, 2000).

Advantages of smeared crack approach:

- Separate interface elements are not needed.
- Crack pattern doesn't need to be known beforehand, which makes this method much more computational friendly.

Disadvantages of smeared crack approach:

- More general method since it indicates cracked regions only.
- Material response, including cracks needs to be smeared out.
- The area over which the crack response should be smeared out needs to be known in advance

When it comes to comparison of both models in practise, discrete crack models have less problems with numerical convergence. Additionally, since separate elements are being used to model the discrete crack a pre-defined crack path is necessary while forming the FE mesh which is a big disadvantage for the designer (Plos, 2000) and (Johansson, 2000).

The material behaviour can be transferred to a stress-strain relation (which is needed in a continuum element) by dividing the crack width with a length, called the crack band width. This concept was introduced by (Bazant & Oh, 1983) and is based on the assumption that the cracks localizes into narrow bands of cracked concrete with uncracked concrete in between. The discrete crack is thus smeared out over the width of the band. Under the condition that the crack band width is one element row wide, the crack band width can be assumed equal to the size of the finite elements. There are three parameters that are being used to describe the fracture properties: Fracture energy, uniaxial strength limit and width of the crack band (Bazant & Oh, 1983).

There are many material models using the smeared crack approach like the fixed crack model and the rotating crack model. In the fixed crack model, the crack orientation is fixed as soon as it is initiated. If the stress state shifts, both normal and shear stresses need to be transferred across the crack plane. In the rotating crack model, the crack direction is instead assumed to follow the principal stress directions. In this case all shear components are zero. This approach is convenient due to practical reasons, since the user is able to directly specify nonlinear stress-strain curves to describe the material response.

The rotating crack model seems to be more advantageous over the fixed crack models regarding the fact that shear across the crack plane and problems associated with that can be avoided (for example stress-locking). This approach however, isn't the only one that is able to bypass this problem. Several other crack models based on plasticity share the same advantage. (Rots, 1988) pointed out that in the rotating crack model when a new crack activates the previous ones are becoming inactive. Eventually we end up with only one active crack. This could be disadvantageous when the process of loading isn't proportional. Despite that the concept of rotating cracks may seem unrealistic, many studies have shown that good results can be obtain with this method, while material models with fixed cracks often gives a too stiff response and overestimates the capacity (Johansson, 2000).

2.2.2 Interaction between reinforcement and concrete

In order to carry loads a reinforced concrete structure needs a good bond between the concrete and reinforcement. The bond stress is dependent on several factors including bar roughness, bar diameter, bar location, bar ending, concrete class, bar anchorage length and direction of concrete casting (Tejchman & Bobinski, 2014). When a reinforcement bar is pulled out of concrete, inclined interior cracks are formed from the top of the ribs. To keep equilibrium, circular tensile hoop stress will form around the bar. When the pulling force becomes large enough, radial stresses extending from the bar will arise. When these cracks reach the concrete surface, a splitting failure will occur.

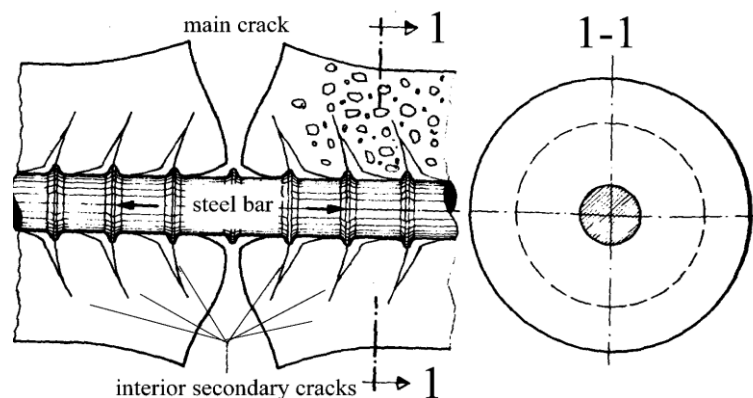


Figure 2.9 Crack formation during tension test of a reinforced concrete prism (Tejchman & Bobinski, 2014).

The material properties of concrete and reinforcement very different. Steel behaves very similar during tensile and compressive tests, unlike concrete which is known for its high compressive but low tensile strength. There is also a huge disproportion in modulus of elasticity of both materials. Concrete cracks for rather low tensile stresses while the reinforcement is still elastic. That causes the need for bond transfer between reinforcement and concrete. Therefore, it is very common to consider these two materials as separate contributors in terms of overall stiffness of the whole structure (Chen, 2007).

The transmission of stresses between reinforcement and concrete is obtained mostly through contact directly between the reinforcement ribs and concrete. When the reinforcement slips relative to the concrete, not only shear stresses, but also normal stresses will be transferred from the bar to the concrete. The normal stresses may cause splitting cracks in the concrete, with loss of bond (or anchorage) capacity as a consequence. To properly describe the phenomenon of bond between reinforcement and concrete, surface interface elements can be introduced. In that case a special interface model needs to be used. The role of this model is to describe the interaction between reinforcement and concrete in the contact zone. It should consist of several factors describing the bond phenomenon including bond stresses and splitting stresses. In practice, if we want to obtain precise stresses in the contact zone which are compatible with experiments, a non-symmetric stiffness matrix needs to be used. Doing so, we allow the normal stresses to be generated thanks to the slip of the bar (Plos, 2000).

2.3 Crack width predictions

2.3.1 Crack widths according to Eurocode 2

In order to have a good understanding of the expected results, a reference value of crack widths is essential. A good starting point to predict the crack widths can be obtained by using equations from (EN 1992-1-1, 2004). Crack width can be calculated using equation (2.7). The method is strongly dependent on the maximum cracking spacing and the mean values of strains in reinforcement and concrete.

$$w_k = s_{r,max}(\varepsilon_{sm} - \varepsilon_{cm}) \quad (2.7)$$

Where:

$s_{r,max}$	Maximum cracking spacing
ε_{sm}	Mean strain in reinforcement under relevant combination loads
ε_{cm}	Mean strain in concrete between cracks

According to (EN 1992-1-1, 2004) maximum cracking spacing can be calculated using two different formulas.

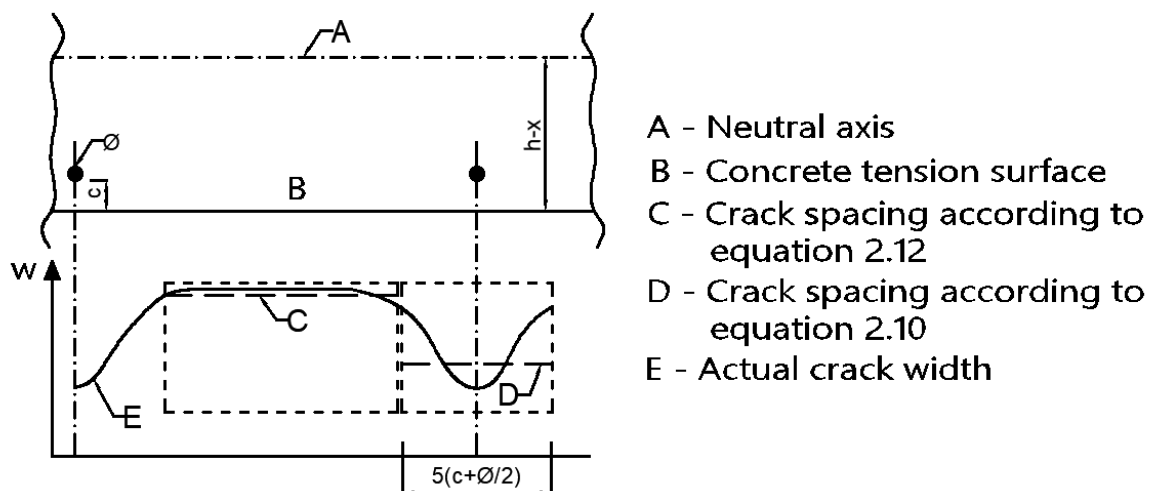


Figure 2.10 Crack width, w , at concrete surface relative to distance from bar based on (EN 1992-1-1, 2004).

If the spacing between the bonded reinforcement in tension meets the criterion:

$$spacing \leq 5 \left(c + \frac{\phi}{2} \right) \quad (2.8)$$

Then the maximum cracking spacing should be calculated using equation:

$$s_{r,max} = k_3 c + k_1 k_2 k_4 \phi / \rho_{p,eff} \quad (2.9)$$

However, the mean crack distance should be calculated using another equation according to (EN 1992-1-1, 2004):

$$s_m = \frac{s_{r,max}}{1.7} \quad (2.10)$$

Where:

c	Is the cover to the longitudinal reinforcement
\emptyset	Bar diameter
k_1	Coefficient which takes into account the bond properties of reinforcement
k_2	Coefficient which takes into account the distribution of strain
$k_2 = 0.5$	<i>for bending</i>
$k_2 = 1.0$	<i>for pure tension</i>
$k_1 = 0.8$	<i>for high bond bars</i>
$k_1 = 1.6$	<i>for bars with an effectively plain surface</i>
$k_3 = 3.4$	<i>Recommended value</i>
$k_4 = 0.425$	<i>Recommended value</i>

If the criterion presented in (2.8) is not met (the spacing of the bonded reinforcement exceeds the value of $5 \left(c + \frac{\emptyset}{2} \right)$ or there doesn't exist bonded reinforcement within the tension zone) then a simplified equation can be used:

$$s_{r,max} = 1.3(h - x) \quad (2.11)$$

Where:

$(h - x)$ is the distance between the neutral axis and concrete tension surface which can be seen in Figure 2.10

The value of $\varepsilon_{sm} - \varepsilon_{cm}$ can be calculated from another equation:

$$\varepsilon_{sm} - \varepsilon_{cm} = \frac{\sigma_s - k_t \frac{f_{ct,eff}}{\rho_{p,eff}} (1 + \alpha_e \rho_{p,eff})}{E_s} \geq 0.6 \frac{\sigma_s}{E_s} \quad (2.12)$$

Where:

σ_s	Stress in tension reinforcement assuming a cracked section
E_s	modulus of elasticity of steel
α_e	Is the ratio $\frac{E_s}{E_{cm}}$
k_t	Is a factor dependent on the duration of the load

A precise calculation of stresses in the reinforcement is important to obtain valid results of the crack widths. However, because of its complicity, some researchers recommend to use simplified formulas during pure bending to avoid additional computational time (Knauff, 2013).

$$\sigma_s = \frac{M}{zA_{s1}} \quad (2.13)$$

Where:

M	Bending moment in a studied cross-section
d	Effective depth of the cross-section
A_{s1}	Cross sectional area of tension reinforcement
$z = 0.80d$	

For more precise predictions, another formula based on (Knauff, 2013) should be taken into consideration:

$$\sigma_s = \alpha_e \frac{M}{I_{II}} (d - x_{II}) \quad (2.14)$$

Where:

x_{II}	Compressive height of a cracked cross-section in state II further described in Figure 2.7.
I_{II}	Moment of inertia in state II
$\alpha_e = \frac{E_s}{E_{cm}}$	

2.3.2 Crack widths according to ACI

The calculations according to ACI 224R are much easier in terms of computational effort compared to Eurocode 2 approach.

$$w = 2 \frac{f_s}{E_s} \beta \sqrt{d_c^2 + \left(\frac{s}{2}\right)^2} \quad (2.15)$$

$$w_m = \frac{w}{1.7} \quad (2.16)$$

Where:

w	Maximum crack width, in. (mm);
w_m	Mean crack width, in. (mm);
f_s	Reinforcing steel stress, ksi (MPa);
E_s	Reinforcing steel modulus of elasticity, ksi (MPa);
d_c	Thickness of cover from tension face to center of closest bar, in. (mm);
s	Bar spacing, in. (mm)
β	Ratio of distance between neutral and tension face to distance between neutral axis and centroid of reinforcing steel

2.4 Multi-level Assessment Strategy

During FE analyses different levels of detailing can be adopted depending on the type of the structure and the expected structural response. A higher level of detailing is not always better, as the computational time raises with the complexity of analysis. Therefore, it is critical to understand what level of detailing is optimal for our needs. It is clear, that with a more detailed assessment we obtain a deeper understanding of our structural response. However, for simple problems it may be that using sophisticated solutions is not necessary because of the poor results compared to the additional work we might put into the model. A Multi-level Assessment Strategy has been developed for reinforced concrete slabs (Plos et al., 2016).

(I) Simplified analysis

In this level of detailing the structural analysis is made with simplified 2D beam element models. From the structural analysis cross-sectional forces and

moments are obtained. The stress in reinforcement is calculated using a simplified state II analysis which is then used in the equations for crack width calculations as described in (point 2.3). The most commonly used models are described in the Eurocode 2 (EN 1992-1-1, 2004) and in national regulations like (ACI Committee 224, 2008).

(II) 3D linear FE analysis

Here, the structural analysis is made with 3D shell FE model. In this analysis some simplifications are used, including linear elastic material response and simplifications in modelling of the geometry. The cross-sectional forces and moments obtained may be necessary to redistribute due to these simplifications. The results can then be used to calculate crack widths in analogous way like in level I.

(III) 3D nonlinear shell FE analysis

At the 3rd level of detailing in the multi-level assessment strategy shell elements and nonlinear analysis are used. The reinforcement is modelled with full bond to the concrete. This level of assessment is used together with local resistance or crack models on higher levels of approximation.

(IV) 3D nonlinear FE analysis with continuum elements and fully bonded reinforcement

A nonlinear FE analysis is performed where concrete is modelled by using 3D continuum elements and reinforcement is fully bonded with the concrete (in a similar way to level III). To obtain a better crack pattern, the reinforcement layers should be modelled in a dense FE mesh.

(V) 3D nonlinear FE analysis with continuum elements including the slip between reinforcement and concrete.

In this level of detailing continuum elements are used to model the concrete and separate elements to model the reinforcement. However, unlike in level IV the bond-slip behavior between reinforcement and concrete is included. A big advantage of this model is that by using a fine mesh it is possible to track single cracks.

2.5 Finite element analysis

While analysing a reinforced concrete under static loading it is common to use incremental and iterative methods to obtain the proper response of the structure. In order to solve the FE problem some assumptions considering initial stiffness are made, however many improvements during the analysis are made until the convergence is obtained with an approximate equilibrium point. One of the most popular iteration methods are the Newton-Raphson and modified Newton-Raphson method. The main difference between these two methods is that the stiffness matrix is updated only once in each increment in the modified method. This means that it requires less work during the iteration process. The response which we obtain during the analysis in case of reinforced concrete structures is usually strongly nonlinear (Plos, 2000).

The reinforcement is embedded in concrete (with a certain cover) in the tensile zone to support concrete in carrying loads. This means that we can typically model the reinforcement as one-dimensional elements which are working in the longitudinal direction. The reinforcement can be modelled in different ways. One of them is to use truss elements with interface elements which imitate the bond-slip behaviour in the contact zone between reinforcement and concrete. Another way is to model the reinforcement embedded in concrete, which means that there is no need of using separate elements. However, while using this technique we assume a complete interaction between the materials. In an even more detailed model 3D continuum elements can be used both for concrete and reinforcement, with an interface model between them (Plos, 2000).

When performing FE analysis of a reinforced concrete structure it is important to pick the appropriate crack stress-strain relation. In a smeared crack model, the crack displacements are divided by a certain length over which the crack is going to be smeared out. Before cracking most of the stresses are carried by concrete. However, once the crack initiates the tensile stresses are being taken by the reinforcement which are then distributed on each side of the crack. However, when using the embedded reinforcement model, where complete interaction is assumed, the forces are transferred directly to the next concrete element. A tension stiffening effect is being introduced in Figure 2.11. The grey shaded area represents the load carried by the reinforcement and the unshaded white area stands for the load carried by concrete. This effect can be implemented into the FE model. When the transfer of stresses between reinforcement and concrete elements is modelled, correctly chooses the higher value of stiffness in this region (assuming that the reinforcement and concrete elements were modelled correctly) (Plos et al., 2017).

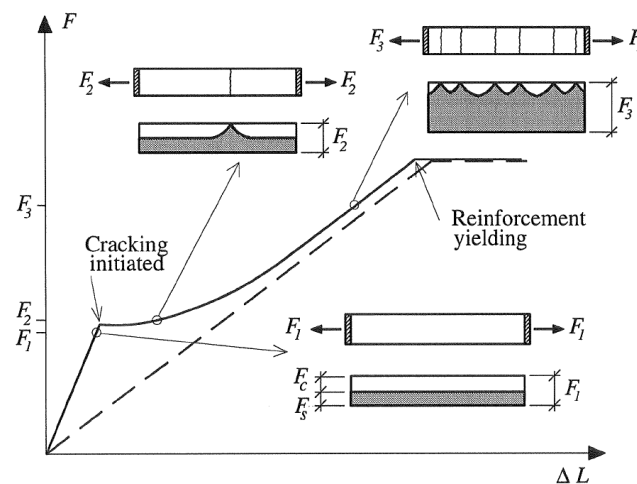


Figure 2.11 Load displacement response of a tensioned reinforced concrete prism (Plos, 2000).

There are multiple advantages of using nonlinear FE analysis instead of the simple linear analysis. One of the main reasons is the fact that a more realistic stress distribution is obtained. The stress concentration is also more accurate and is not as high as using the simple linear analysis. This usually is reflected with more realistic predictions when it comes to structural elements capacity and material response. Nonlinear analysis is becoming nowadays more popular and its application in practice is increasing, mainly because of its realistic results.

During the FE analysis using the smeared crack approach it is necessary to use the stress-strain relation instead of stress-crack opening relation. Therefore, transformation of $(\sigma - w)$ into $(\sigma - \varepsilon_{cr})$ is typically made by dividing the crack opening with the crack band width as:

$$\varepsilon_{cr} = \frac{w_d}{h_b} \quad (2.17)$$

Where:

w_d Crack opening deformation of one crack
 h_b Crack band width (length over which the crack localises)

For different detailing levels in the FE model the crack band width can be given different values:

- a) Plain concrete: $h_b = l_{elem}$
- b) Embedded reinforcement: $h_b = s_{rm}$
- c) Separate reinforcement + steel/concrete slip: $h_b = l_{elem}$

Where:

l_{elem} Length of the FE element
 s_{rm} Mean crack distance

During FE modelling there are several important choices which will influence the obtained results. Therefore, it's important to make the right choices dependent on the level of detailing that is being used. The most important aspects that a designer needs to take into account are:

- Boundary conditions
- Used element types
- Interaction between reinforcement and concrete
- Modelling of details
- Material models and input
- Load
- Mesh

Upon deciding on what kind of elements will be used in the model, it is critical to know what kind of results are expected and important for the work. Beam elements are good to use while describing bending and bending failure, however they cannot describe the failure due to shear. Shell elements are also good to use for describing bending and can characterize the shear failure in plane for some cases. Solid elements are the most complex and in general take more computational time. Many elements are needed over the height of the structural element to properly describe bending with 1st order element, which means that a dense FE mesh is needed.

It is also good to understand how a non-linear FE analysis is done in theory. A step-wise iterative solution is performed. Within each increment an equilibrium needs to be preserved. The analysis is performed until a sufficient approximation is found and the convergence requirements are met. One of the most common iteration methods are the Regular Newton-Raphson presented in Figure 2.12 in which the stiffness is updated within each iteration and Modified Newton-Raphson shown in Figure 2.13 where the stiffness is updated just once in each increment (Plos, 2000).

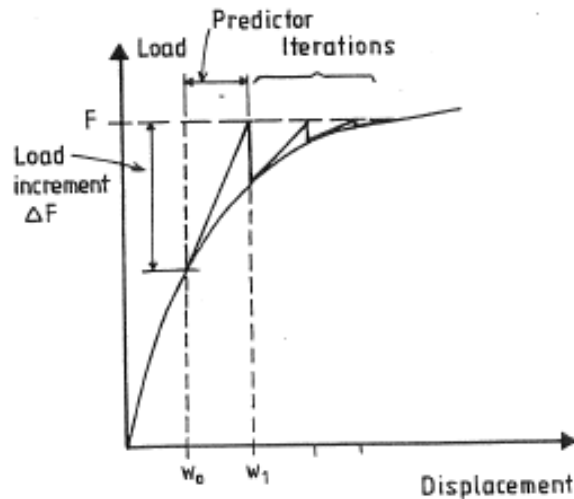


Figure 2.12 Regular Newton-Raphson iteration method (Plos, 2000).

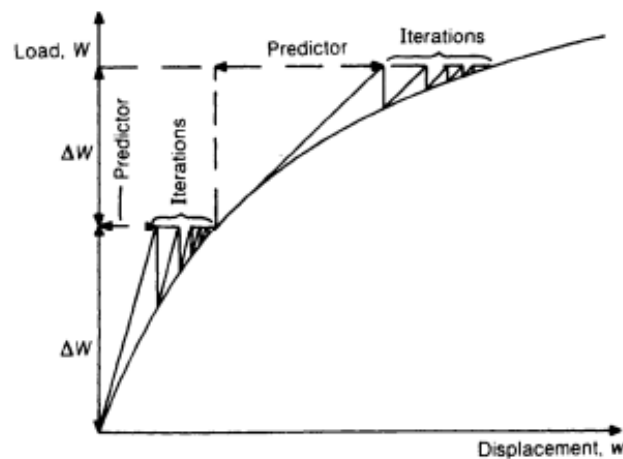


Figure 2.13 Modified Newton-Raphson iteration method (Plos, 2000).

2.6 Previous research

Previously, there were several other researchers who tried to deal with the problem of predicting crack widths. Most of their work however, concerned analytical calculus or linear FE analysis with comparison to experimental results. (Oh & Kim, 2007) presented a method which could be used to accurately predict crack widths for reinforced concrete beams under repeated loads. During their work they pointed out that including bond stress-slip relation is essential in order to obtain realistic results. To perform their experiments, they used four-point bending tests on reinforced concrete beams which were subjected to monotonic loading. The results in the form of crack widths were acquired by crack gauges with microscopes. Later on, their results were compared with well-known codes such as (ACI Committee 224, 2008) and Euro-National Concrete Committee (1990) as well as with more complicated formulas presented by other researchers. The comparison showed that there exists a big scatter between the experimental tests and (ACI Committee 224, 2008) and Euro-National Concrete Committee (1990) however using equation (2.18) presented by (Balazs, 1993) gives accurate prediction.

$$w = 2 \left(\frac{s_{p1}^\alpha \emptyset (1 + \alpha)}{8(1 + n_E \rho_{s,eff}) \tau_{max} E_s} \frac{f_{s2}^2}{(d - c)} \right)^{1/(1+\alpha)} \frac{(h - c)}{(d - c)} \quad (2.18)$$

Where:

h	Height of the flexural member; d – effective depth of reinforcing bars
c	Neutral axis depth
s_{p1}	Slip corresponding to bond strength
τ_{max}	Bond strength
\emptyset	Reinforcing bar diameter
α	Powers in bond stress-slip relations
E_s	Modulus of elasticity of steel
n_E	Modular ratio E_s/E_c
$\rho_{s,eff}$	Effective reinforcement ratio
f_{s2}	Reinforcing bar stress at crack

Another approach, considering nonlinear analysis of crack widths in reinforced concrete structures was carried out by (Tammo et al., 2009). In their work they compare the nonlinear FEM model with former experimental results carried out on axially loaded reinforced concrete prisms with different values of concrete cover and its influence on the crack width. They obtained similar results from the nonlinear FE analysis as for the crack widths measured from the experimental tests. This could indicate that performing nonlinear analyses to predict the crack widths in SLS is possible and should be studied further.

More studies concerning crack width analysis using numerical methods were performed by (Kwan & Ma, 2016). In their recent work they developed a discrete crack model used for crack width analysis. In order to simulate the bond-slip behaviour they introduce interface elements between the concrete elements and bar elements for the reinforcement. In order to verify their theoretical results, they compared three sets of specimens including smooth bars and deformed bars which were tested by other researchers. The experiments showed that the method is likely to overestimate the number of cracks and the spacing between the cracks. When it comes to the crack widths, besides comparing them with the experimental results, they were also compared to predictions based on (ACI Committee 224, 2008) and (EN 1992-1-1, 2004). It was shown that the experimental results matched with the FE results within 7% error. It was also noted that the calculated analytical crack widths based on (ACI Committee 224, 2008) were closer to the FE model predictions than the predictions made from (EN 1992-1-1, 2004) which tended to overestimate the crack width.

3 Experiment description

In order to investigate the possibility to predict the crack widths, three-point bending experimental tests results were used. In this thesis, measurement results from static beam tests made by (Lozano & Makdesi, 2017) were used. In total 6 reinforced concrete beams with concrete from two different batches have been subjected to static loading to investigate the propagation of the cracks (Table 3.1). Additionally, to have a good understanding of the cracking process and to measure the crack widths a camera was positioned in front of the station to record the experiment at rate of 0.5 frames per second (fps) during the test by (Lozano & Makdesi, 2017). To obtain a good contrast and have a better track of the crack propagation the beams were painted with a black pattern on one of the sides which was exposed towards the camera during the experiment. As a part of the current master thesis, the data was processed using Digital Image Correlation (DIC), with the software GOM Correlate Professional.

Table 3.1 Numbering of the beams subjected to three-point bending experiments.

Load type	Beam no.	Batch	Cross-section area [mm ²]	Total length [mm]	Reinforcement
Three-point bending	B-07, B-08, B-09	1	10000	1180	4Ø6
	B-16, B-17, B-18	2	10000	1180	4Ø6

Besides three-point bending, several other tests have been made in order to specify the material properties. Specifically, there were over 9 concrete cube specimens to determine the most important properties of concrete and 7 specimens of reinforcing steel which were tested in order to determine the strength of the steel used.

3.1 Beam geometry and material properties

Figure 3.1 shows the geometry of reinforced concrete beams which were used during the three-point bending static tests. The cross-section of the beam is a square with the dimensions 100 x 100 mm. Four reinforcement bars of a diameter 6 mm (4Ø6) were placed symmetrically in each corner of the beam. The concrete cover of the bars was equal to 17 mm.

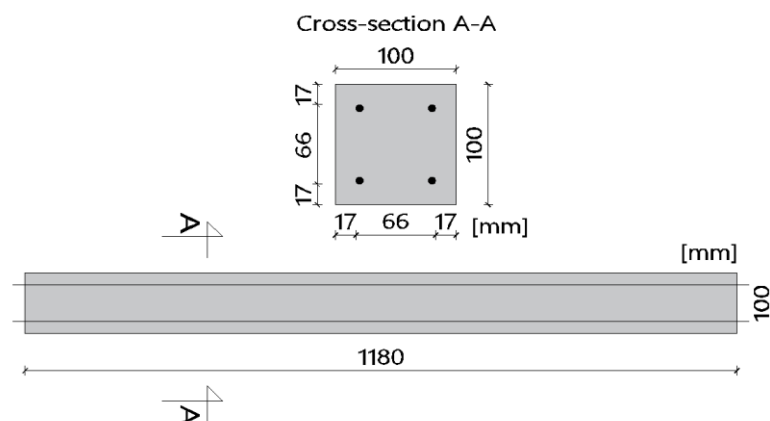


Figure 3.1 Geometry of the beams tested.

During casting of the reinforced concrete beams observations were made, regarding the difference in diameters of the reinforcement in different cross-sections which varied from 5 – 6 mm. Another observation was that due to a small diameter of the bars, the reinforcement did not perfectly stay in its intended position all along the specimen during casting of the concrete, but was bending due to self-weight and the weight of the poured concrete. The main reason for this was that no rebar spacers were used to increase the stability and stiffness of the longitudinal bars and even though transverse hangers were used to prevent this problem, they were not sufficient to perfectly keep the reinforcement in place. The moulds were carefully cleaned and greased before casting in a similar manner.

3.1.1 Concrete properties

Concrete properties were determined from static standard tests done at 36 days (Batch 1 and Batch 2) after casting. The testing included determining the compressive and tensile strength, density and the fracture energy of the specimens and was performed in accordance to Swedish standards (CEN, 2009) and recommendations given in (Löfgren et al., 2004). In total, 9 cubic specimens with a 150 mm nominal dimension were tested. Mean values of the material properties have been calculated which were used in this study.

All the mean values of the tested concrete specimens have been summarized in Table 3.2. It is also worth mentioning that the values have been recalculated from cube specimens (which are very common in Sweden) into more international values coming from cylinder specimens using approximative equations (3.1) and (3.2). Afterwards, modulus of elasticity for concrete was estimated by using equation (3.3). However, alternatively, other approximative methods could have been used to estimate the modulus of elasticity of concrete (for example using the almost linear relation between stress and strain shown in (

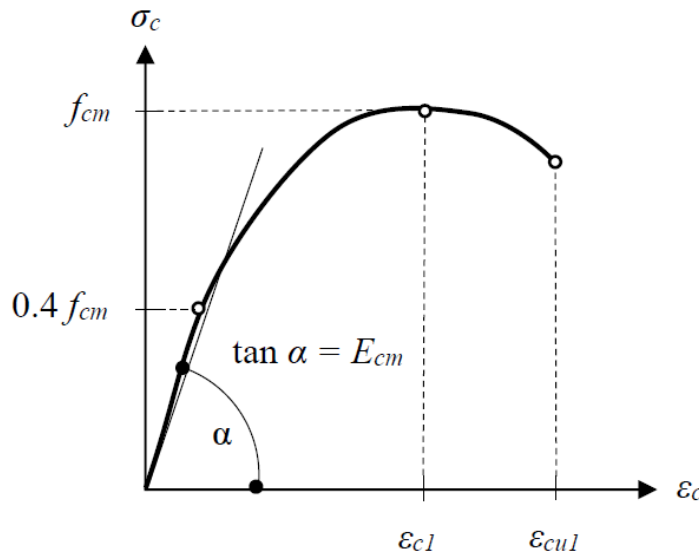


Figure 3.2) which gives similar results.

$$f_{cm} = 0.8 f_{cm, cube} \text{ [MPa]} \quad (3.1)$$

$$f_{ct} = 0.9 f_{ct, sp} \text{ [MPa]} \quad (3.2)$$

Where:

f_{cm}	Mean value of concrete cylinder compressive strength
$f_{cm,cube}$	Mean value of concrete cube compressive strength
f_{ct}	Axial tensile strength of the specimen
$f_{ct,sp}$	Splitting tensile strength of the specimen

$$E_{cm} = 22 \left(\frac{f_{cm}}{10} \right)^{0.3} \text{ [GPa] and } (f_{cm} \text{ in MPa}) \quad (3.3)$$

Where:

E_{cm}	Secant modulus of elasticity of concrete
----------	--

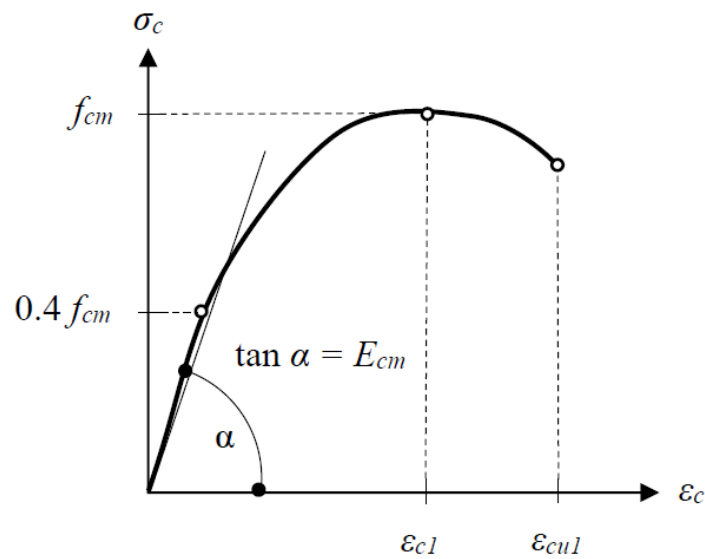


Figure 3.2 Schematic relation of stresses and strain for concrete analyses (EN 1992-1-1, 2004).

Table 3.2 Average values of concrete properties obtained by recalculating the values measured on cube specimens into corresponding values for cylindric specimens (Lozano & Makdesi, 2017).

Property	Description	Average values from three-point bending tests	Unit
$f_{cm,36}$	Mean compressive strength after 36 days	42.2	[MPa]
$f_{ctm,36}$	Mean tensile strength after 36 days	3.7	[MPa]
G_f	Fracture energy	132.0	[Nm/m ²]
$E_{cm,36}$	Modulus of elasticity after 36 days	33.9	[GPa]

3.1.2 Steel properties

The steel material properties were obtained by performing tensile tests in a universal testing machine. Additionally, in order to get a very precise value of modulus of elasticity, special equipment in the form of an extensometer was used to obtain the

proper values of strains. All the averaged values of steel properties are displayed in Table 3.3. These values are further used in this thesis.

Table 3.3 Average values of reinforcing steel properties in experimental tests by (Lozano & Makdesi, 2017).

Property	Description	Average values from three-point bending tests	Unit
f_u	Ultimate stress	686	[MPa]
$f_{0.2}$	Proof stress	575	[MPa]
E_s	Young's Modulus	196	[GPa]
ε_{su}	Ultimate strain	10.8	[%]

It was also noted that the steel behavior and its properties were rather similar to a cold-worked steel. When analyzing this type of steel, it is very common to use the mean value of proof stress instead of yield strength which is more suitable for hot rolled steel.

3.2 Static tests procedure

The static tests which were performed by (Lozano & Makdesi, 2017) concerned testing of reinforced concrete beams which are labelled in this thesis as Batch 1 and Batch 2. The supports were located symmetrically to keep the distance of 1000 mm of the beam span. The load was subjected directly in the middle of the span in the form of a point load. The static tests were interrupted when one of the two following criteria were fulfilled:

- The failure of one of the reinforcement bars was reached.
- The applied load was reduced to approximately 70% of the maximum load in the post peak response.

A set of two cameras and spotlights was used to record the experiment. They were placed symmetrically on both sides in front of the station pointing from an angle to the mid span of the beam. The recording rate was 0.5 fps. The camera setup is shown in Figure 3.5. (Lozano & Makdesi, 2017)

3.2.1 Three-point bending tests

Tests on the reinforced concrete beams from Batch 1 and Batch 2 (see Table 3.1) were performed 35 and 36 days after casting, respectively. Figure 3.3 and Figure 3.4 show the schematic and actual representation of the deformation controlled static three-point bending tests, respectively. Based on the material properties it could be noted that the scatter between the maximum and minimum value of proof stress of steel was equal to 5% and the scatter between the maximum and minimum value of compressive strength of concrete was equal to 11%. Therefore, the mean values of the material properties both for concrete and steel were used.

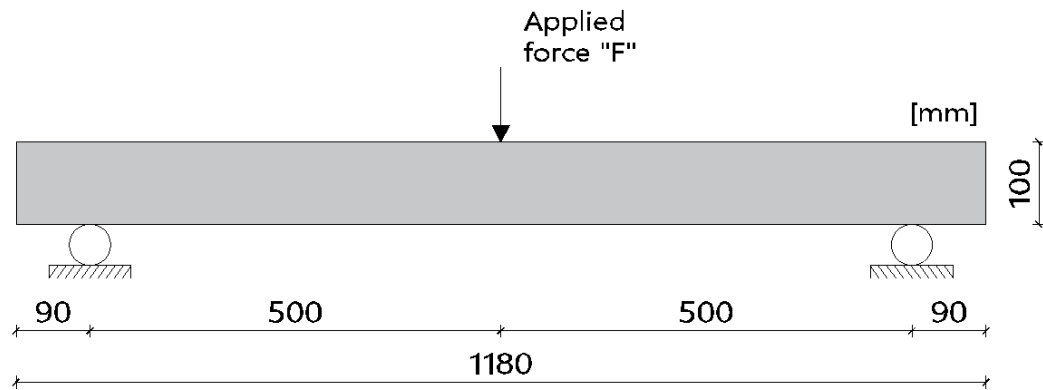


Figure 3.3 Schematic setup for static tests – Three-point bending experiment on Batch 1 and Batch 2.



Figure 3.4 Station setup for the static tests: Three-point bending experiment on Batch 1 and Batch 2 (Lozano & Makdesi, 2017).

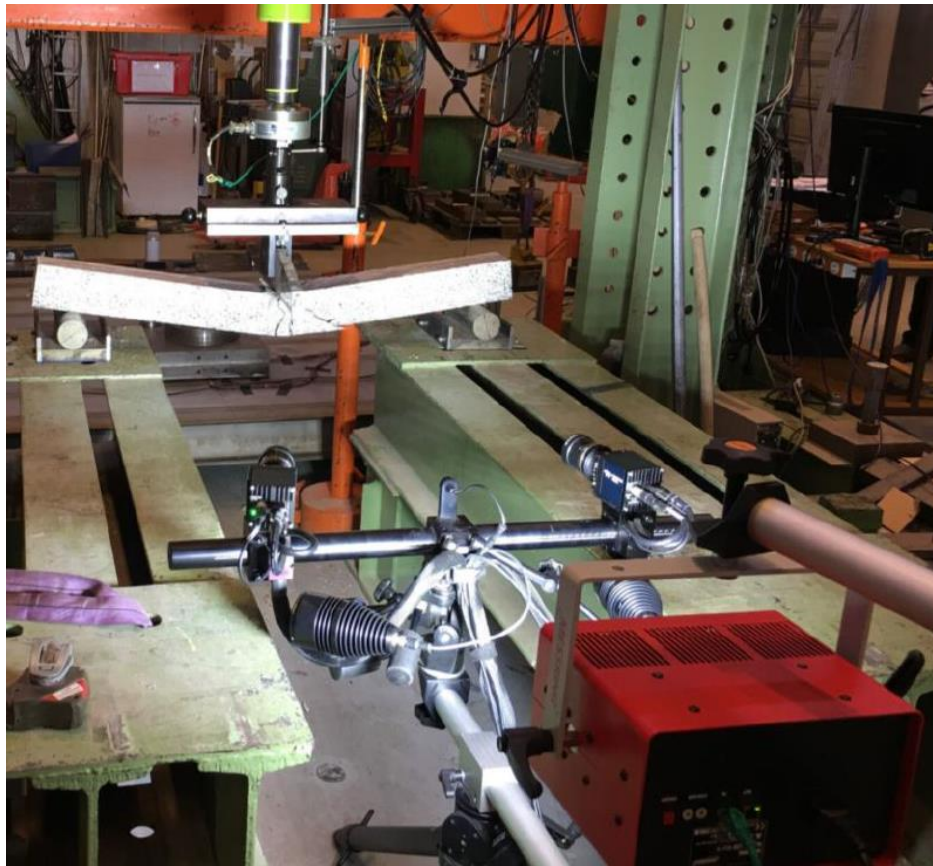


Figure 3.5 Camera setup for the static tests: Three-point bending experiment on Batch 1 and Batch 2 (Lozano & Makdesi, 2017).

3.3 Digital Image Correlation

DIC is an optical system which can be used to measure relative displacements both in 2D, using one camera or in 3D, while using a set of two cameras. The system works by tracking the movement and matching together facets on the object in several following images. To trace displacements in 3D, it finds and calculates the coordinates from both cameras and correlates them together. This information is then used to measure the displacements. In this way the system is able to calculate the, deformation and strains in corresponding points throughout the test.

It is very important to properly prepare the specimen before testing. To do so, a pattern should be painted on the surface of the structure, covering approximately 50% of the area to create a good contrast for the cameras. After performing the experiment, a certain field which is captured by the cameras is being analysed. It is possible to create experiments on small and big structures. However, when analysing big structures, a good system calibration is needed. It is also worth mentioning that DIC is an approximate method and it is common to have certain deviations. Although it is not possible to obtain the same accuracy for a single point as when using sophisticated equipment like extensometers, a good optical image of the whole field studied is captured which is very practical, user friendly and easily comparable with the results coming from Eurocode 2 calculations.

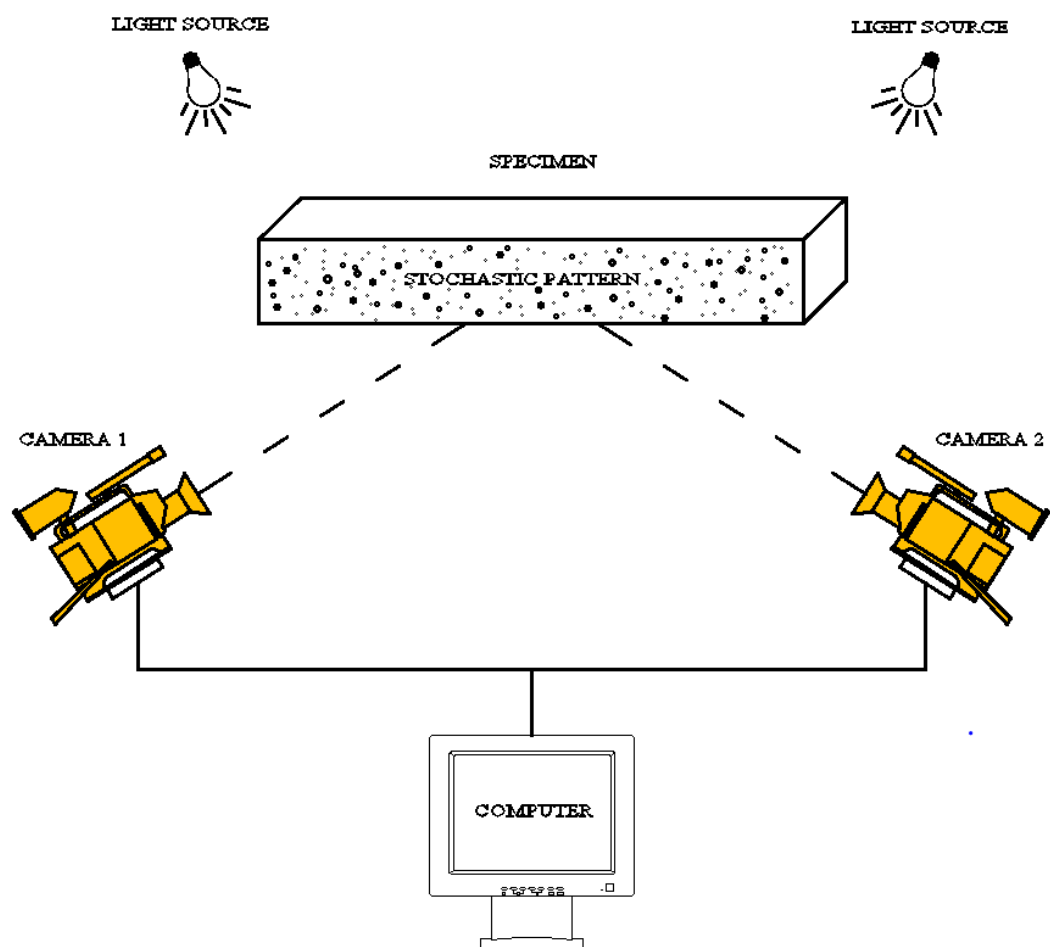


Figure 3.8 Schematic representation of DIC during experiments.

4 Comparison of results

In this chapter comparison between experimental results and theoretical predictions from (EN 1992-1-1, 2004) and (ACI Committee 224, 2008) is performed. Three-point bending tests results are presented in this thesis.

4.1 General

In Figure 4.1 and Figure 4.2 force-displacement relation and its envelope are shown. Based on the averaged value marked as dotted line in Figure 4.3 it can be observed, that reinforcing steel starts to yield at a force equal to approximately 11 kN and the highest peak of the force reaches approximately 14 kN.

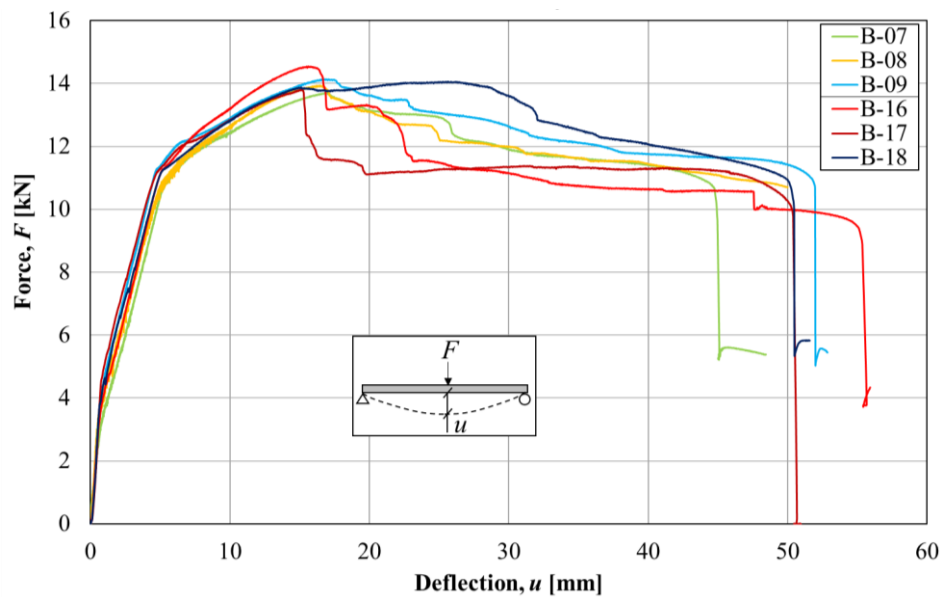


Figure 4.4 Force-displacement diagram during three-point bending static test based on (Lozano & Makdesi, 2017).

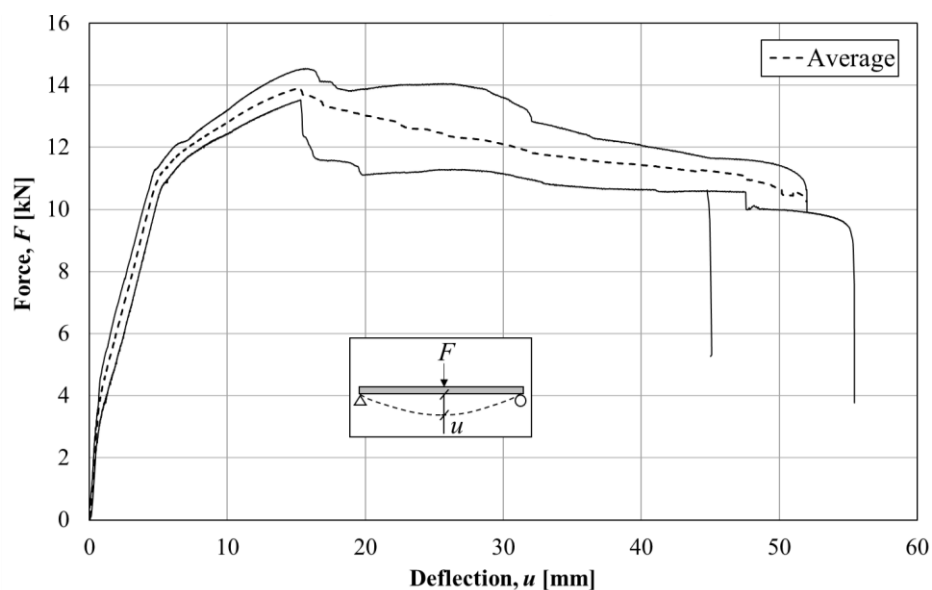


Figure 4.5 Outer envelopes and average values of Force-Displacement diagrams based on (Lozano & Makdesi, 2017).

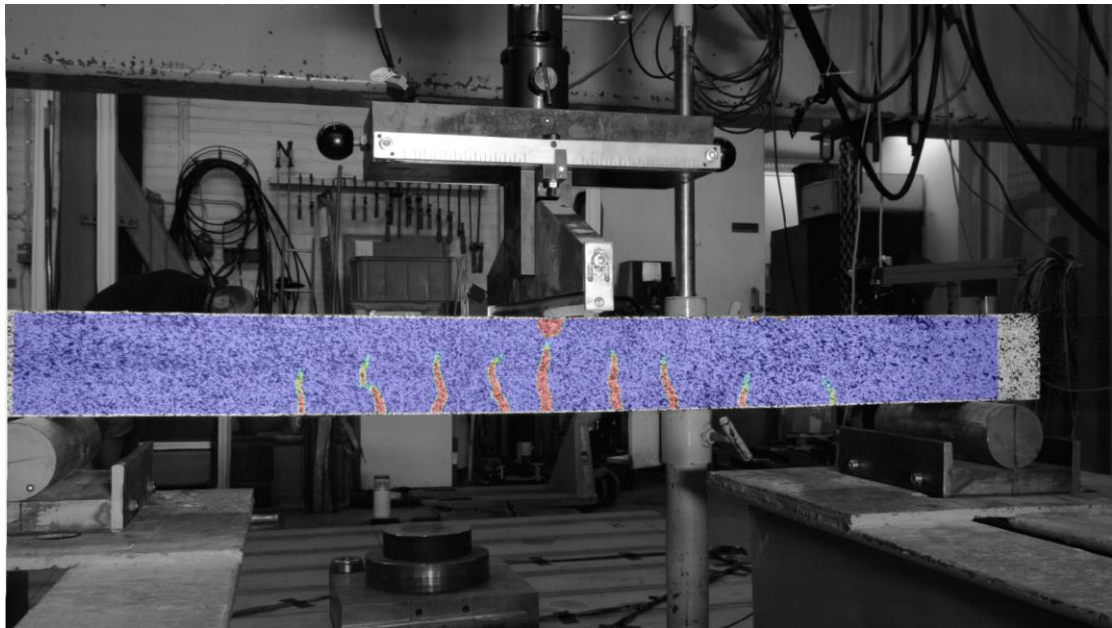


Figure 4.6 Left camera view of the strain field from DIC.

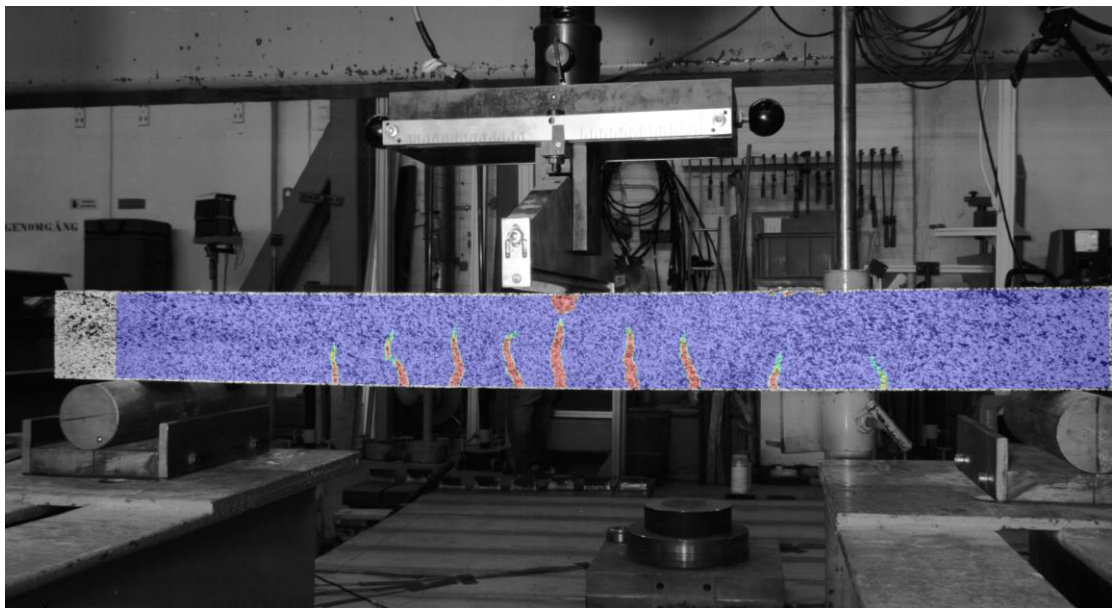


Figure 4.7 Right camera view of the strain field from DIC.

Figure 4.6 and Figure 4.7 represent a typical beam specimen and its strain field at a load equal to 11 kN. A view both from left camera and right camera is presented. DIC is capturing only the mid-span between the supports of the beam equal to 1 meter. The outer parts of the beam are out of interest and are not displayed.

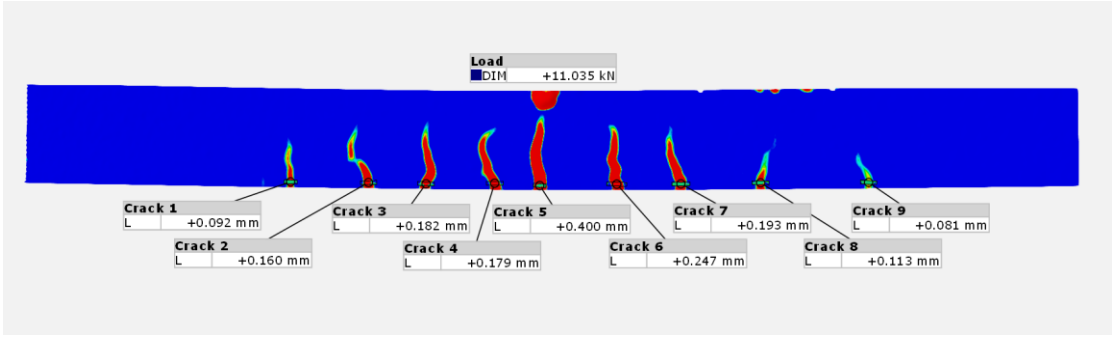
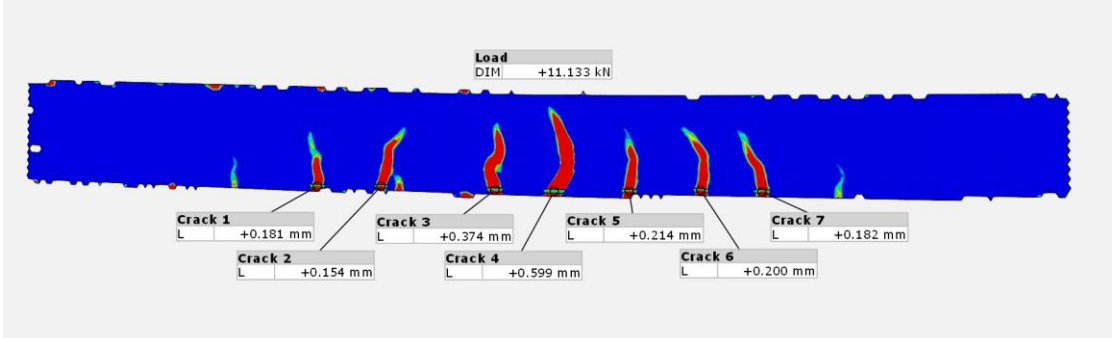
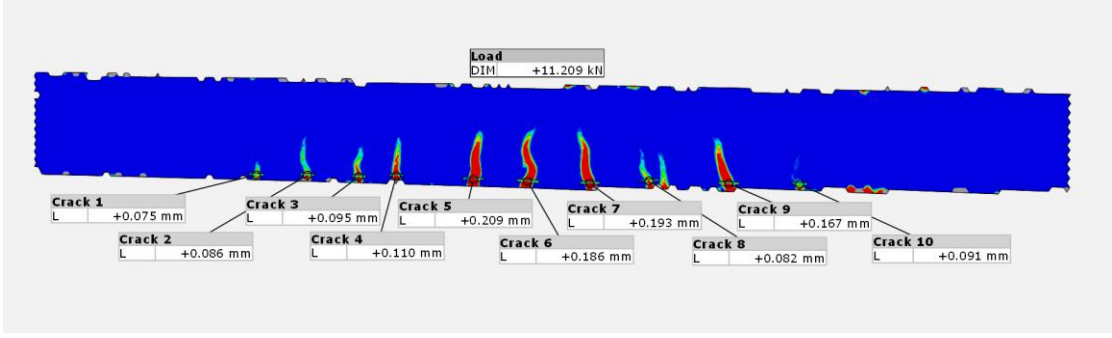
Three-point bending tests	Batch 1 Beams																						
 <p>Load DIM +11.035 kN</p> <table border="1"> <thead> <tr> <th>Crack</th> <th>Width (mm)</th> </tr> </thead> <tbody> <tr><td>Crack 1</td><td>+0.092</td></tr> <tr><td>Crack 2</td><td>+0.160</td></tr> <tr><td>Crack 3</td><td>+0.182</td></tr> <tr><td>Crack 4</td><td>+0.179</td></tr> <tr><td>Crack 5</td><td>+0.400</td></tr> <tr><td>Crack 6</td><td>+0.247</td></tr> <tr><td>Crack 7</td><td>+0.193</td></tr> <tr><td>Crack 8</td><td>+0.113</td></tr> <tr><td>Crack 9</td><td>+0.081</td></tr> </tbody> </table>	Crack	Width (mm)	Crack 1	+0.092	Crack 2	+0.160	Crack 3	+0.182	Crack 4	+0.179	Crack 5	+0.400	Crack 6	+0.247	Crack 7	+0.193	Crack 8	+0.113	Crack 9	+0.081	B-07		
Crack	Width (mm)																						
Crack 1	+0.092																						
Crack 2	+0.160																						
Crack 3	+0.182																						
Crack 4	+0.179																						
Crack 5	+0.400																						
Crack 6	+0.247																						
Crack 7	+0.193																						
Crack 8	+0.113																						
Crack 9	+0.081																						
 <p>Load DIM +11.133 kN</p> <table border="1"> <thead> <tr> <th>Crack</th> <th>Width (mm)</th> </tr> </thead> <tbody> <tr><td>Crack 1</td><td>+0.181</td></tr> <tr><td>Crack 2</td><td>+0.154</td></tr> <tr><td>Crack 3</td><td>+0.374</td></tr> <tr><td>Crack 4</td><td>+0.599</td></tr> <tr><td>Crack 5</td><td>+0.214</td></tr> <tr><td>Crack 6</td><td>+0.200</td></tr> <tr><td>Crack 7</td><td>+0.182</td></tr> </tbody> </table>	Crack	Width (mm)	Crack 1	+0.181	Crack 2	+0.154	Crack 3	+0.374	Crack 4	+0.599	Crack 5	+0.214	Crack 6	+0.200	Crack 7	+0.182	B-08						
Crack	Width (mm)																						
Crack 1	+0.181																						
Crack 2	+0.154																						
Crack 3	+0.374																						
Crack 4	+0.599																						
Crack 5	+0.214																						
Crack 6	+0.200																						
Crack 7	+0.182																						
 <p>Load DIM +11.209 kN</p> <table border="1"> <thead> <tr> <th>Crack</th> <th>Width (mm)</th> </tr> </thead> <tbody> <tr><td>Crack 1</td><td>+0.075</td></tr> <tr><td>Crack 2</td><td>+0.086</td></tr> <tr><td>Crack 3</td><td>+0.095</td></tr> <tr><td>Crack 4</td><td>+0.110</td></tr> <tr><td>Crack 5</td><td>+0.209</td></tr> <tr><td>Crack 6</td><td>+0.186</td></tr> <tr><td>Crack 7</td><td>+0.193</td></tr> <tr><td>Crack 8</td><td>+0.082</td></tr> <tr><td>Crack 9</td><td>+0.167</td></tr> <tr><td>Crack 10</td><td>+0.091</td></tr> </tbody> </table>	Crack	Width (mm)	Crack 1	+0.075	Crack 2	+0.086	Crack 3	+0.095	Crack 4	+0.110	Crack 5	+0.209	Crack 6	+0.186	Crack 7	+0.193	Crack 8	+0.082	Crack 9	+0.167	Crack 10	+0.091	B-09
Crack	Width (mm)																						
Crack 1	+0.075																						
Crack 2	+0.086																						
Crack 3	+0.095																						
Crack 4	+0.110																						
Crack 5	+0.209																						
Crack 6	+0.186																						
Crack 7	+0.193																						
Crack 8	+0.082																						
Crack 9	+0.167																						
Crack 10	+0.091																						

Figure 4.8 Numbering of cracks and crack widths from DIC tests – Batch 1, at a load level of about 11 kN.

Views of the strain fields for all the specimens are displayed in Figure 4.8 and Figure 4.9. The red parts indicate the cracks appearing. One facet point on either side of the crack at the level of reinforcement, were defined for each crack and the horizontal deformations between the facet points were measured to obtain precise values of the crack widths with increasing load on the beam.

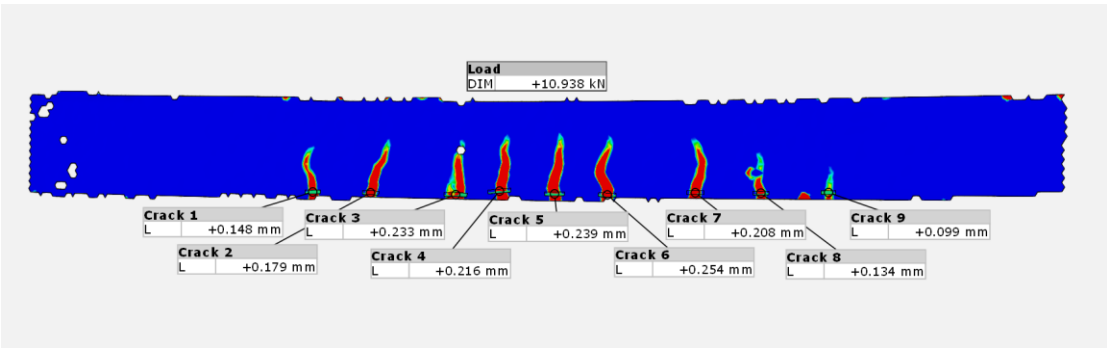
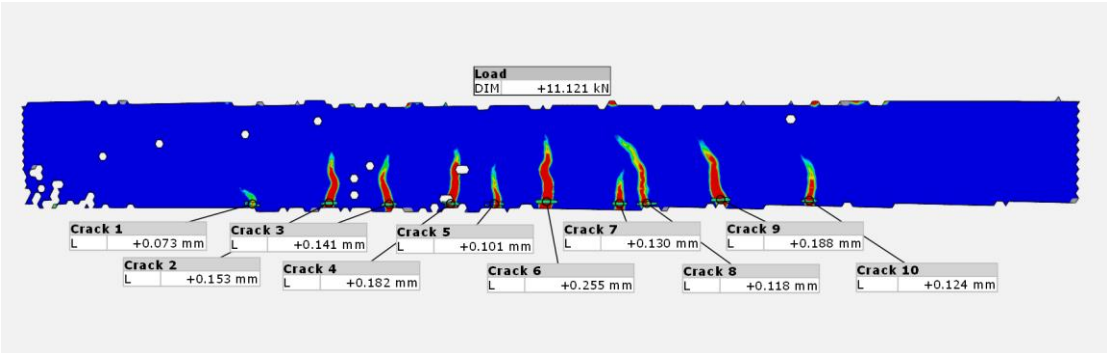
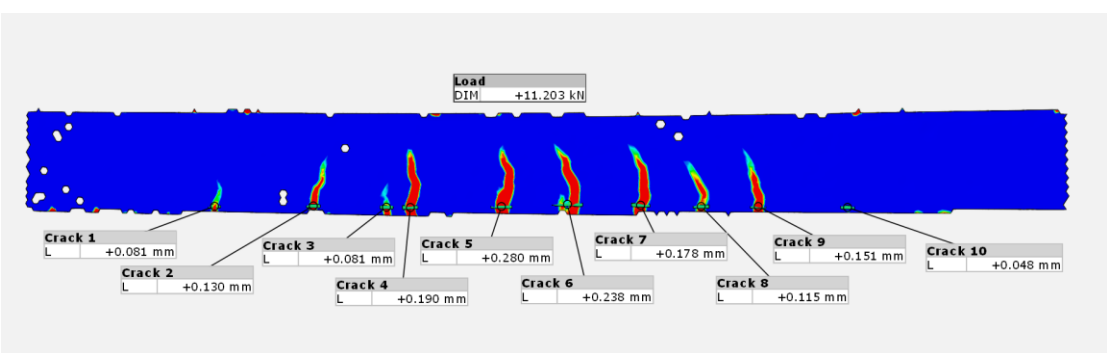
Three- point bending tests	Batch 2 Beams																						
 <p>Load DIM +10.938 kN</p> <table border="1"> <thead> <tr> <th>Crack</th> <th>Width (mm)</th> </tr> </thead> <tbody> <tr><td>Crack 1</td><td>+0.148</td></tr> <tr><td>Crack 2</td><td>+0.179</td></tr> <tr><td>Crack 3</td><td>+0.233</td></tr> <tr><td>Crack 4</td><td>+0.216</td></tr> <tr><td>Crack 5</td><td>+0.239</td></tr> <tr><td>Crack 6</td><td>+0.254</td></tr> <tr><td>Crack 7</td><td>+0.208</td></tr> <tr><td>Crack 8</td><td>+0.134</td></tr> <tr><td>Crack 9</td><td>+0.099</td></tr> </tbody> </table>	Crack	Width (mm)	Crack 1	+0.148	Crack 2	+0.179	Crack 3	+0.233	Crack 4	+0.216	Crack 5	+0.239	Crack 6	+0.254	Crack 7	+0.208	Crack 8	+0.134	Crack 9	+0.099	B-16		
Crack	Width (mm)																						
Crack 1	+0.148																						
Crack 2	+0.179																						
Crack 3	+0.233																						
Crack 4	+0.216																						
Crack 5	+0.239																						
Crack 6	+0.254																						
Crack 7	+0.208																						
Crack 8	+0.134																						
Crack 9	+0.099																						
 <p>Load DIM +11.121 kN</p> <table border="1"> <thead> <tr> <th>Crack</th> <th>Width (mm)</th> </tr> </thead> <tbody> <tr><td>Crack 1</td><td>+0.073</td></tr> <tr><td>Crack 2</td><td>+0.153</td></tr> <tr><td>Crack 3</td><td>+0.141</td></tr> <tr><td>Crack 4</td><td>+0.182</td></tr> <tr><td>Crack 5</td><td>+0.101</td></tr> <tr><td>Crack 6</td><td>+0.255</td></tr> <tr><td>Crack 7</td><td>+0.130</td></tr> <tr><td>Crack 8</td><td>+0.118</td></tr> <tr><td>Crack 9</td><td>+0.188</td></tr> <tr><td>Crack 10</td><td>+0.124</td></tr> </tbody> </table>	Crack	Width (mm)	Crack 1	+0.073	Crack 2	+0.153	Crack 3	+0.141	Crack 4	+0.182	Crack 5	+0.101	Crack 6	+0.255	Crack 7	+0.130	Crack 8	+0.118	Crack 9	+0.188	Crack 10	+0.124	B-17
Crack	Width (mm)																						
Crack 1	+0.073																						
Crack 2	+0.153																						
Crack 3	+0.141																						
Crack 4	+0.182																						
Crack 5	+0.101																						
Crack 6	+0.255																						
Crack 7	+0.130																						
Crack 8	+0.118																						
Crack 9	+0.188																						
Crack 10	+0.124																						
 <p>Load DIM +11.203 kN</p> <table border="1"> <thead> <tr> <th>Crack</th> <th>Width (mm)</th> </tr> </thead> <tbody> <tr><td>Crack 1</td><td>+0.081</td></tr> <tr><td>Crack 2</td><td>+0.130</td></tr> <tr><td>Crack 3</td><td>+0.081</td></tr> <tr><td>Crack 4</td><td>+0.190</td></tr> <tr><td>Crack 5</td><td>+0.280</td></tr> <tr><td>Crack 6</td><td>+0.238</td></tr> <tr><td>Crack 7</td><td>+0.178</td></tr> <tr><td>Crack 8</td><td>+0.115</td></tr> <tr><td>Crack 9</td><td>+0.151</td></tr> <tr><td>Crack 10</td><td>+0.048</td></tr> </tbody> </table>	Crack	Width (mm)	Crack 1	+0.081	Crack 2	+0.130	Crack 3	+0.081	Crack 4	+0.190	Crack 5	+0.280	Crack 6	+0.238	Crack 7	+0.178	Crack 8	+0.115	Crack 9	+0.151	Crack 10	+0.048	B-18
Crack	Width (mm)																						
Crack 1	+0.081																						
Crack 2	+0.130																						
Crack 3	+0.081																						
Crack 4	+0.190																						
Crack 5	+0.280																						
Crack 6	+0.238																						
Crack 7	+0.178																						
Crack 8	+0.115																						
Crack 9	+0.151																						
Crack 10	+0.048																						

Figure 4.9 Numbering of cracks and crack widths from DIC tests – Batch 2, at a load level of about 11 kN.

White dots, which can be seen especially in specimens B-16, B-17 and B-18 indicate the loss of information in these points. However, does not affect the results in most of the cases, because the majority of lost information is located outside the appearing cracks. An exception is specimen B-17 where the information is lost directly in the cracking area of one of the cracks. This will be further discussed later.

As expected, the largest cracks appeared in the middle section of the beam, where the cross-sectional stresses were the highest. The crack pattern was similar with some differences due to the statistical distribution of the material properties and the load step which was not always the same in each beam. Similarities in the tested specimens can be also seen where in most cases 9 to 10 cracks appear before reaching yielding of steel.

4.2 Crack spacing

The crack spacing was measured at the level of reinforcement using DIC. The measurement was done two times with different reference points to make sure that the accuracy of the crack spacing was as high as possible. One of the reference points was located at the left support of the beam, and the second one at the loading point. The difference between measurements using these points was not larger than 5mm in any case, which gave a sufficiently precise overview of the crack positioning.

A schematic view of the cracks which appeared during three-point bending tests can be seen in Figure 4.10 and Figure 4.11. In the figures, diamond markings represent the supports of the beams, square markings represent the start and end of the beam respectively, triangle markings represent the main cracks in the middle of the beam and round markings represent the cracks appearing in the beam. The results are presented for Batch 1 and Batch 2 beams respectively.

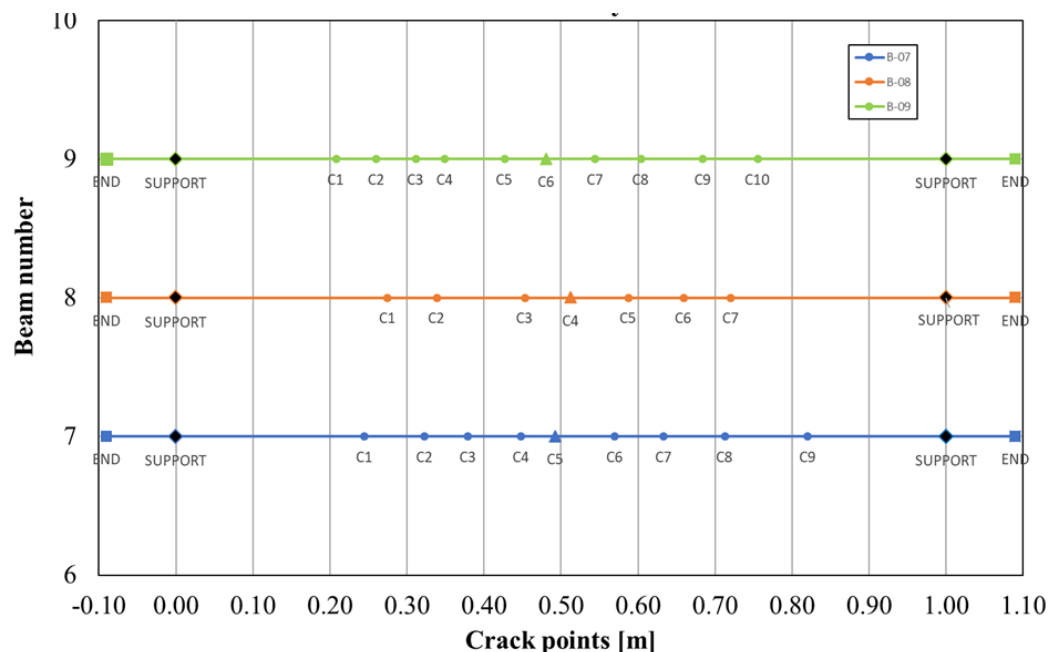


Figure 4.10 Crack spacing from three-point bending tests – Batch 1.

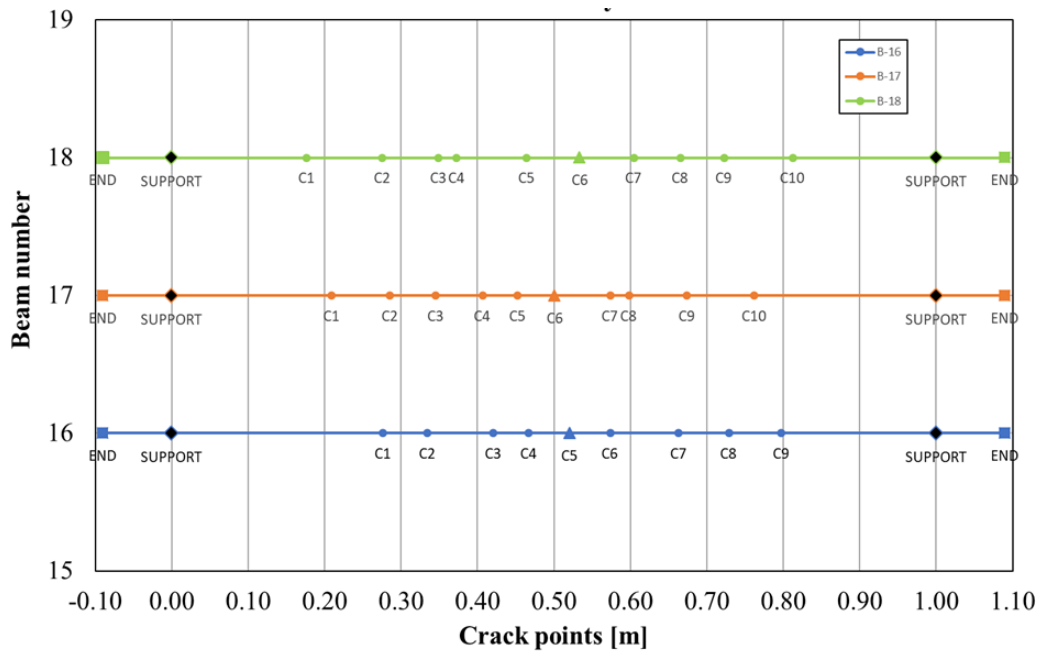


Figure 4.11 Crack spacing from three-point bending tests – Batch 2.

Table 4.1 Maximum and average values of crack spacing obtained during three-point bending tests – Batch 1 and Batch 2.

BATCH 1				BATCH 2			
CRACK SPACING	BEAM B-07 [mm]	BEAM B-08 [mm]	BEAM B-09 [mm]	CRACK SPACING	BEAM B-16 [mm]	BEAM B-17 [mm]	BEAM B-18 [mm]
C1-C2	78	64	52	C1-C2	58	76	99
C2-C3	57	114	52	C2-C3	86	60	74
C3-C4	69	59	38	C3-C4	47	61	24
C5-C6	45	75	78	C5-C6	54	46	92
C6-C7	76	72	54	C6-C7	53	49	70
C7-C8	64	-	63	C7-C8	89	72	70
C8-C9	79	-	60	C8-C9	66	25	61
C9-C10	-	-	80	C9-C10	-	76	57
s_{max}	79	114	80	s_{max}	89	76	99
s_m	67	77	60	s_m	65	58	68
AVERAGE s_m	68			AVERAGE s_m	64		

The maximum crack spacing according to Eurocode 2 was calculated to be $s_{max} = 106$ mm which gives the mean value of crack spacing $s_m = \frac{s_{max}}{1.7} = 62$ mm.

Table 4.1 shows the maximum and average values of crack spacing in the reinforced concrete beams. The values which were marked red are the minimum and maximum values of crack spacing which appeared in all of the tested beams. Comparing the average values, from all the beams, it can be seen that a good prediction of crack spacing was obtained by Eurocode 2. Also, the maximum crack spacing, that appeared in B-08 between Crack 2 and Crack 3 in the experiments was well predicted by the Eurocode 2 approach.

4.3 Crack widths

By using the force measured in the tests, it would be possible to compare the widths of the main cracks which appear in the middle section of the beam directly as a function of the applied force. Figure 4.12 shows the reinforcement stress – crack width relation after first converting the force into the sectional moment of the mid-span and then recalculating this to the reinforcement stress in each cracked section.

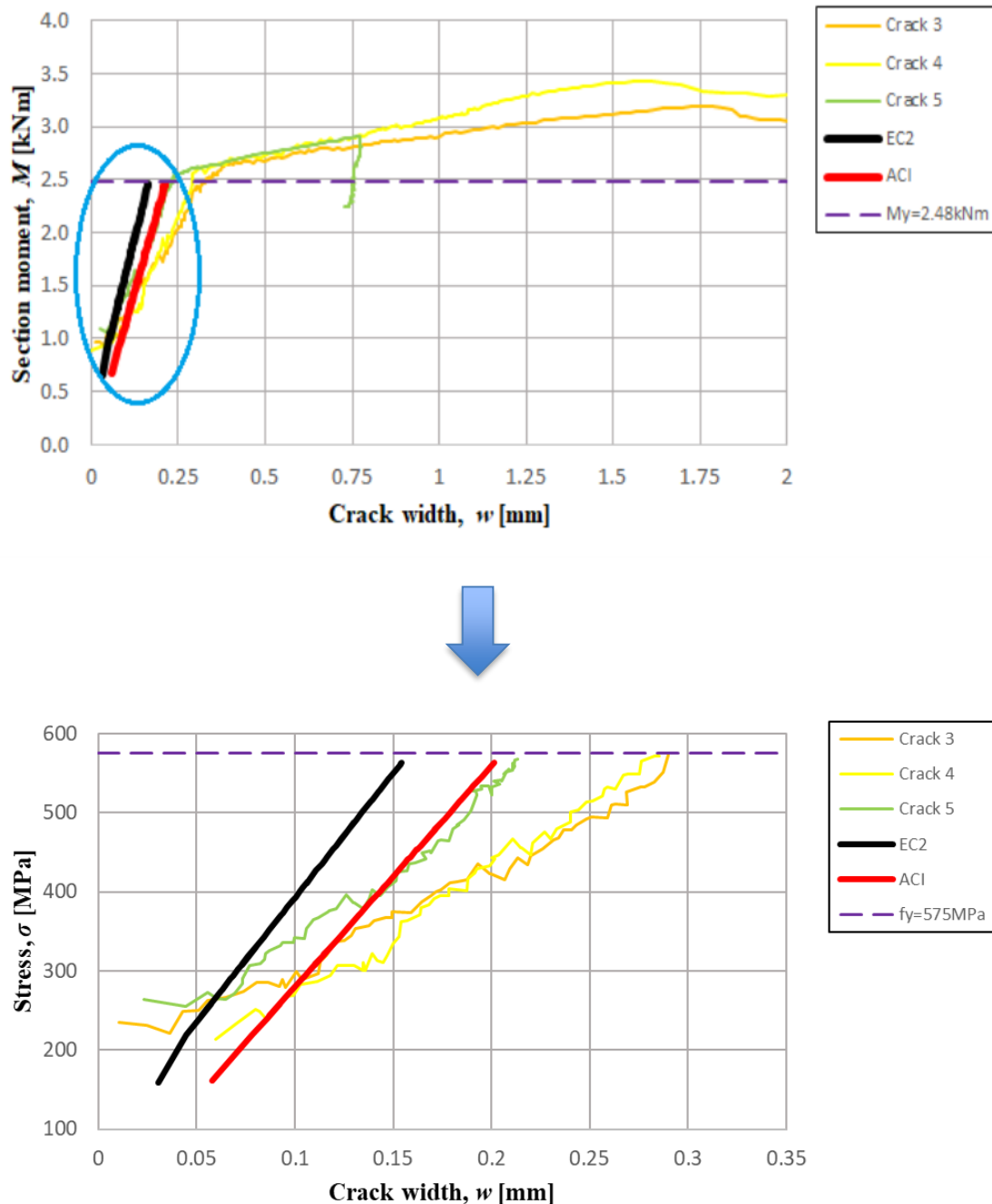


Figure 4.12 Section moment – Mean crack width diagram transformed to Stress – Crack width diagram presented up till reaching yield stress.

It is then possible to determine reinforcement stress-crack opening relations for all cracks which appeared in one specific beam in different cross-sections of the beam.

The stress-crack opening relation can be compared for different cross-sections and to corresponding relations according to Eurocode 2 and ACI 224R. It should be noted that Eurocode 2 and ACI 224R predictions are shown for mean crack width, i.e. they were not divided by 1.7 to obtain the characteristic value of crack widths. This thesis focuses mainly on Serviceability Limit States. Therefore, the reinforcement stress was calculated assuming linear response of the cracked section in State II i.e. yielding of the reinforcement steel is assumed not to be reached. All of the diagrams below are presented in a similar manner.

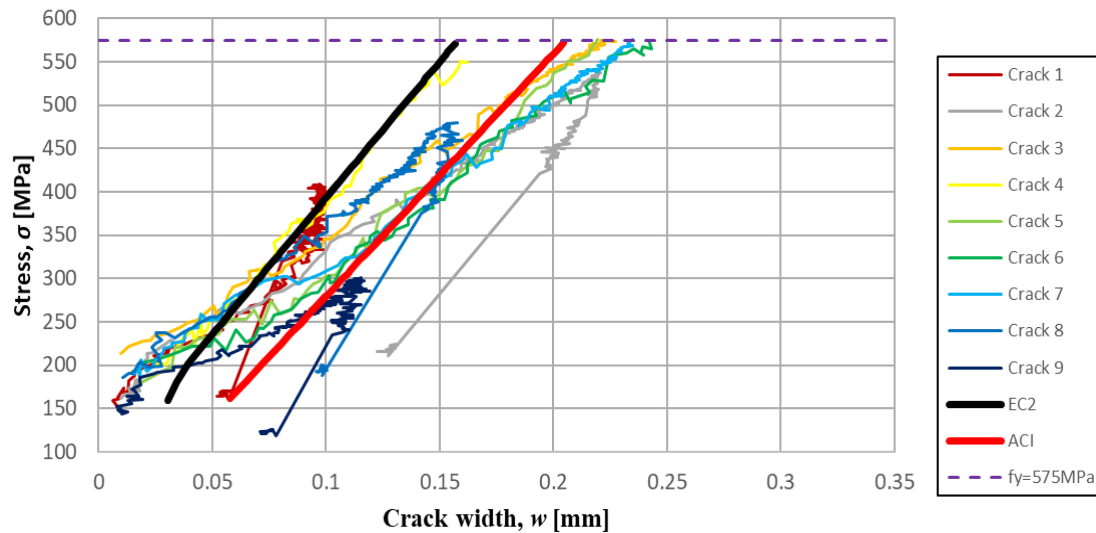


Figure 4.13 Reinforcement stress – Mean crack width diagram for BEAM B-07 before reaching yield stress.

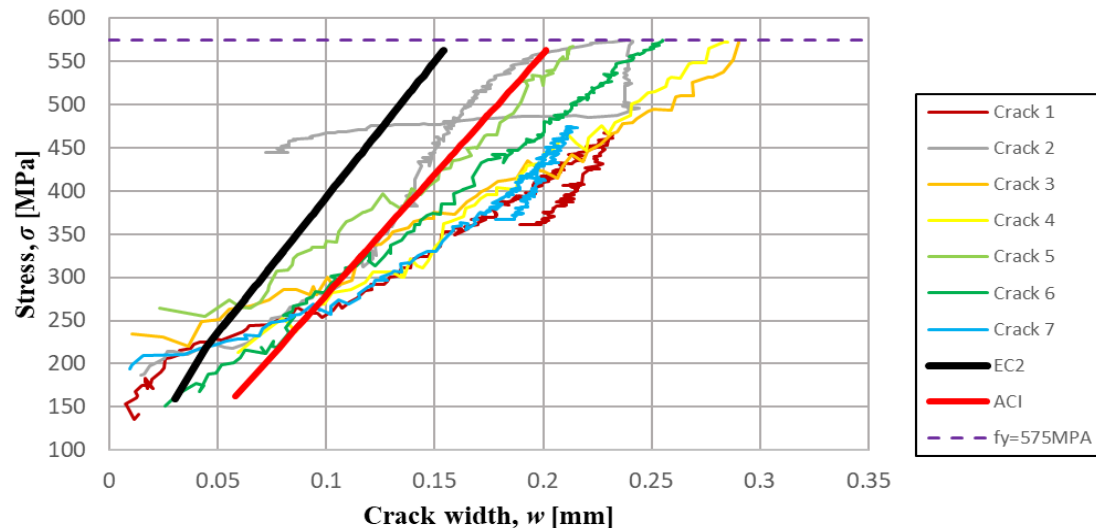


Figure 4.14 Reinforcement stress – Mean crack width diagram for BEAM B-08 before reaching yield stress.

Figure 4.13 to Figure 4.18 show the reinforcement stress-crack opening relations for all cross-sections of the beams where cracking appeared. For each crack the reinforcement stress has been calculated for the corresponding cross-section. All of

the results are presented for stresses up to yield stress. Results for stresses higher than the yield stress (state III) are not shown since a nonlinear analysis would be required to determine the stress. The graphs are shown only after noise stabilization of the measurements, this was reached when the measured crack widths reached a value of at least 0.01 mm.

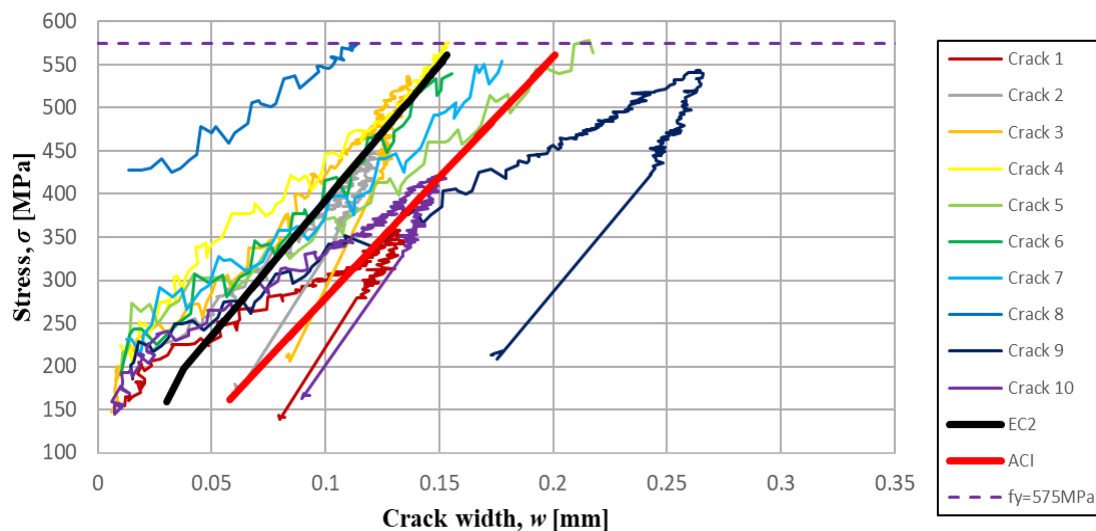


Figure 4.15 Reinforcement stress – Mean crack width diagram for BEAM B-09 before reaching yield stress.

According to Figure 4.8 there are two small cracks next to each other at Crack 8. The two small cracks together form a crack width which could explain why Crack 8 is so small in Figure 4.15.

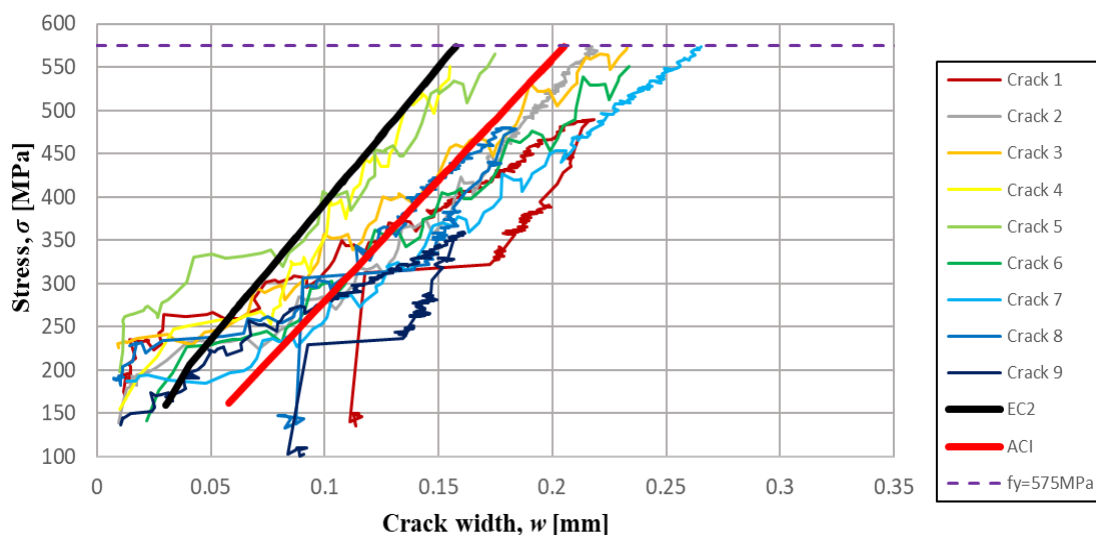


Figure 4.16 Reinforcement stress – Mean crack width diagram for BEAM B-16 before reaching yield stress.

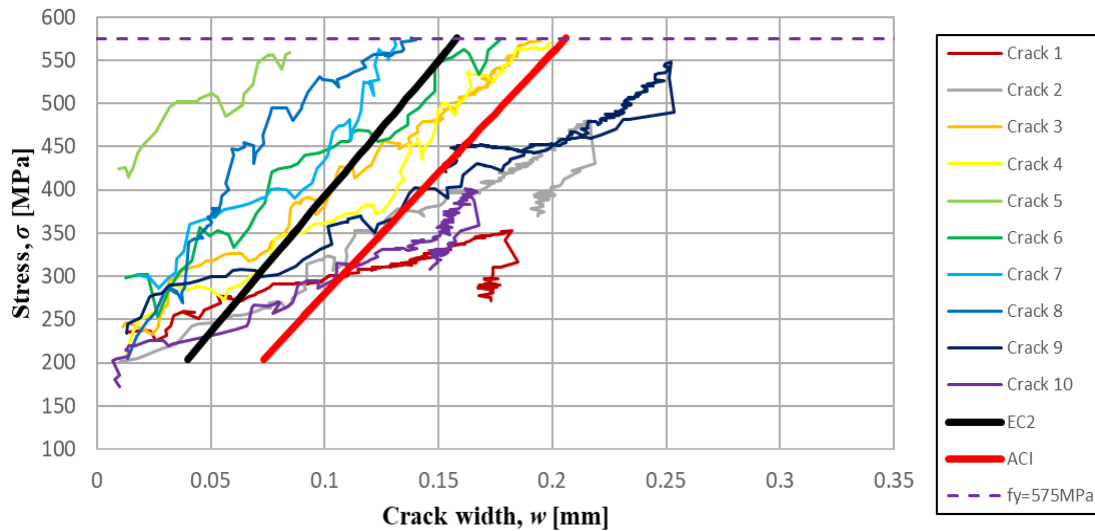


Figure 4.17 Reinforcement stress – Mean crack width diagram for BEAM B-17 before reaching yield stress.

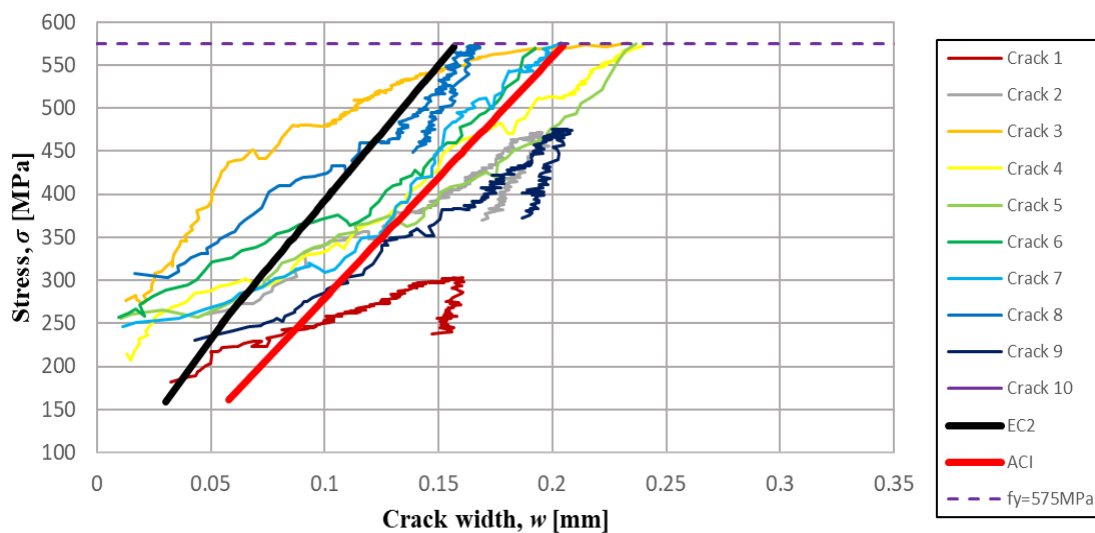


Figure 4.18 Reinforcement stress – Mean crack width diagram for BEAM B-18 before reaching yield stress.

For most of the beams, Eurocode 2 gives a quite good and safe estimation of the crack width for small reinforcement stresses. However, after reaching a reinforcement stress equal to approximately 260MPa we can see that it starts to underestimate the crack width. ACI 224R gives more conservative prediction.

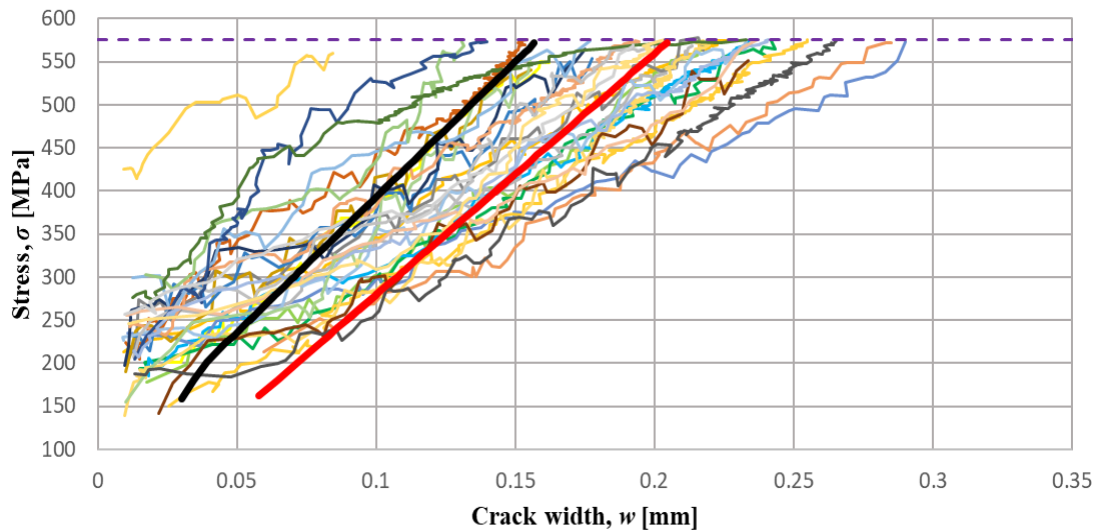


Figure 4.19 Reinforcement stress – Mean crack width diagram for propagating cracks before reaching yield stress for all of the beams.

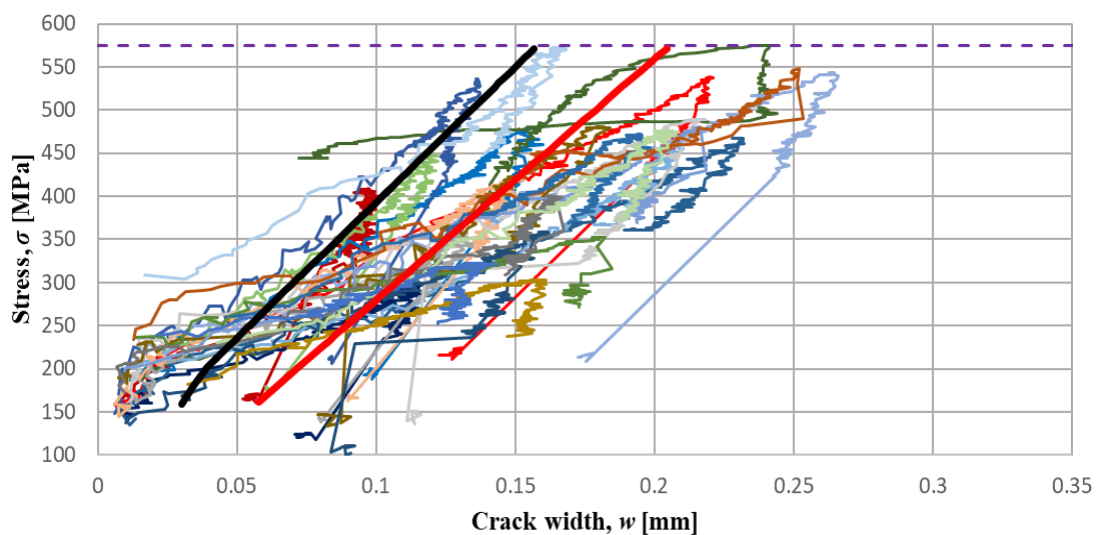


Figure 4.20 Reinforcement stress – Mean crack width diagram for closing cracks before reaching yielding stress for all of the beams.

To examine the results further, they were divided into propagating cracks (Figure 4.19) and closing cracks (Figure 4.20):

- Propagating crack are the cracks in which the reinforcement reached the yield stress during the experiment.
- Closing cracks are the cracks in which the reinforcement never reached the yield stress. These cracks can therefore be plotted throughout the whole duration of experiment.

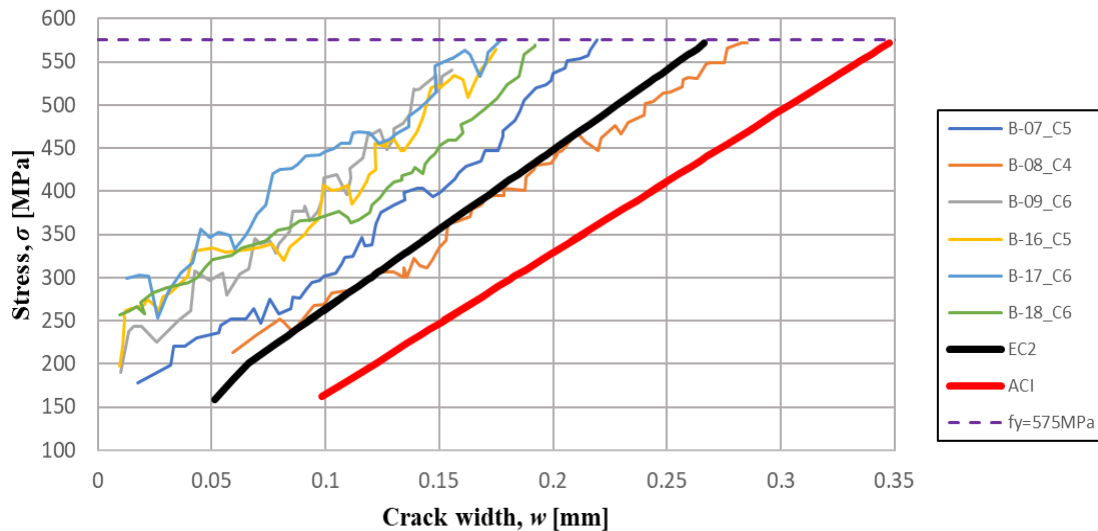


Figure 4.21 Reinforcement stress – Characteristic crack width diagram for main cracks in the middle section of the beams before reaching the yield stress value

For propagating cracks in Figure 4.19, we can see that Eurocode 2 gives a quite good estimation of the crack widths since its stress-crack width relation seems to be located somewhat in the middle between the smallest and largest crack widths measured. A more conservative, however still not perfect prediction is obtained using ACI 224R. Since the mean crack width values are of interest, a prediction in between the two approaches would be even better for the propagating cracks. The situation is similar for the closing cracks, Figure 4.20. Here Eurocode 2 slightly underestimates the crack widths and ACI gives a more conservative prediction.

Figure 4.21 shows the reinforcement stress – characteristic crack width relation only for the main cracks situated directly in the middle of the beam. It should be noted that the Eurocode 2 prediction and ACI 224R values in this specific case were not divided by 1.7 factor to keep the characteristic value of crack widths. We can see that Eurocode 2 is almost on point with its prediction giving a very precise estimation for the characteristic crack width whereas ACI 224R tends to overestimate the crack width.

5 Conclusions

5.1 General conclusions

The general aim of this thesis was to deepen the knowledge and understanding of how DIC can be used for verification of the calculated crack widths and how precise the predictions in common calculation methods are compared to experimental results from earlier studies.

For maximum crack widths estimation, EC 2 gives very precise prediction, whereas ACI 224R slightly overestimates the results. Comparing the calculated maximum crack spacing and the mean crack spacing according to EC 2 with the measurements it can be noted that they correspond well to each other. The theoretical and experimental values vary from each other not more than 8 mm for the maximum crack spacing and 4mm for the mean values which gives a good estimation. The obtained crack patterns from the experiments were similar with small differences. In most of the beams, 9 to 10 cracks appeared before reaching the yield stress of steel. For mean crack widths EC 2 tends to overestimate the crack widths especially in the beginning phase of crack propagation up to approximately 260 MPa of steel stress. However, above that stress level, EC 2 seems to give an accurate prediction of mean crack widths. ACI 224R strongly overestimates the mean crack width during the beginning phase of the crack propagation and slightly overestimates the crack width in later stage of crack propagation, giving a conservative prediction. When analyzing the widest characteristic crack widths (main cracks) in the beams only, which is usually the case in the engineering practice, it is clear that EC 2 gives a close prediction whereas ACI 224R gives a conservative prediction.

For all of the cracks which appeared in different cross-sections of the beams tested, a reinforcement stress-crack width relation was determined. In this way, a large amount of results was gained and a good overview of the crack propagation in SLS could be seen. A large amount of data is needed to get a good view of the statistical distribution of the cracks.

DIC is a powerful method to process optical images which is used to effectively measure crack widths on a surface of a test specimen without using locally attached measuring equipment. It gives precise results after reaching noise stabilization and a good general overview of the whole element studied. However, good system calibration and high resolution of the cameras is required to obtain satisfying results. Additionally, special preparation of the specimen is required beforehand, which can be time consuming. GOM Correlate Professional is a powerful and simple software which is used for the evaluation of 3D surfaces. By creating a strain field for the whole structure, it gives a good track of crack propagation within each load step.

5.2 Future studies

To provide a full range of recommendations for evaluation of crack width predictions additional studies should be performed. There is a need to study how well crack widths can be predicted using non-linear FE analysis on different levels of detailing, performed according to the Multi-level Assessment Strategy described in point 2.4. During modelling, specific material models should be taken into

account both for reinforcement and concrete. The geometry of the beam, boundary conditions and deformation-controlled loading alongside with the self-weight of the beam should be applied in a way that is reflecting the experiments. The FEM results could then be compared with DIC measurements. A full bond between reinforcement and concrete and shell elements should be used while creating one of the models. Then, while creating another model the bond-slip relation between reinforcement and concrete and continuum elements should be implemented. In this way the influence of bond-slip relation and the usage of different types of elements could be studied by comparing the results on different levels of detailing within the measured values from DIC.

In this thesis only experiments on beams with small square cross-section 100 x 100 mm were studied. Therefore, there is a need to perform experiments on specimens with larger cross-sections to compare the results with beams in another scale, to see if there exists a size effect. Additionally, longer spans of the beams, different amounts of reinforcement and beams with transverse reinforcement could be tested. The reinforcing steel properties used in this thesis were somewhat similar to cold worked steel. By using a typical hot-rolled steel with a clear plastic region it would be possible to use a precise value obtained from the experiments of the yield stress instead of the approximately determined proof stress.

Other load settings could also be considered. In this thesis, only three-point bending tests were studied. This means that the distribution of stresses was almost linearly decreasing from the peak point to the supports. By including other load settings like four-point bending, the middle section of the beam would have an almost constant value of bending moments. This could possibly have an impact on the received crack pattern in the beams and hopefully give more similar crack widths located in the middle section of the beam, which would be much easier to study on the same stress level. Having a more stable bending moment diagram could also influence the DIC measurement. By studying the area where the bending moments are constant only, a better resolution of the cameras could be obtained which would give more precise measurements. Additionally, by using four-point instead of three-point bending, local crushing of concrete would be avoided in the loading point.

Additionally, other approaches to evaluate the crack widths could be studied in addition to the ones in EC 2 and ACI 224R. Finally, higher resolution cameras and other lightning set-ups could be tested to see how better equipment influences the results obtained.

6 References

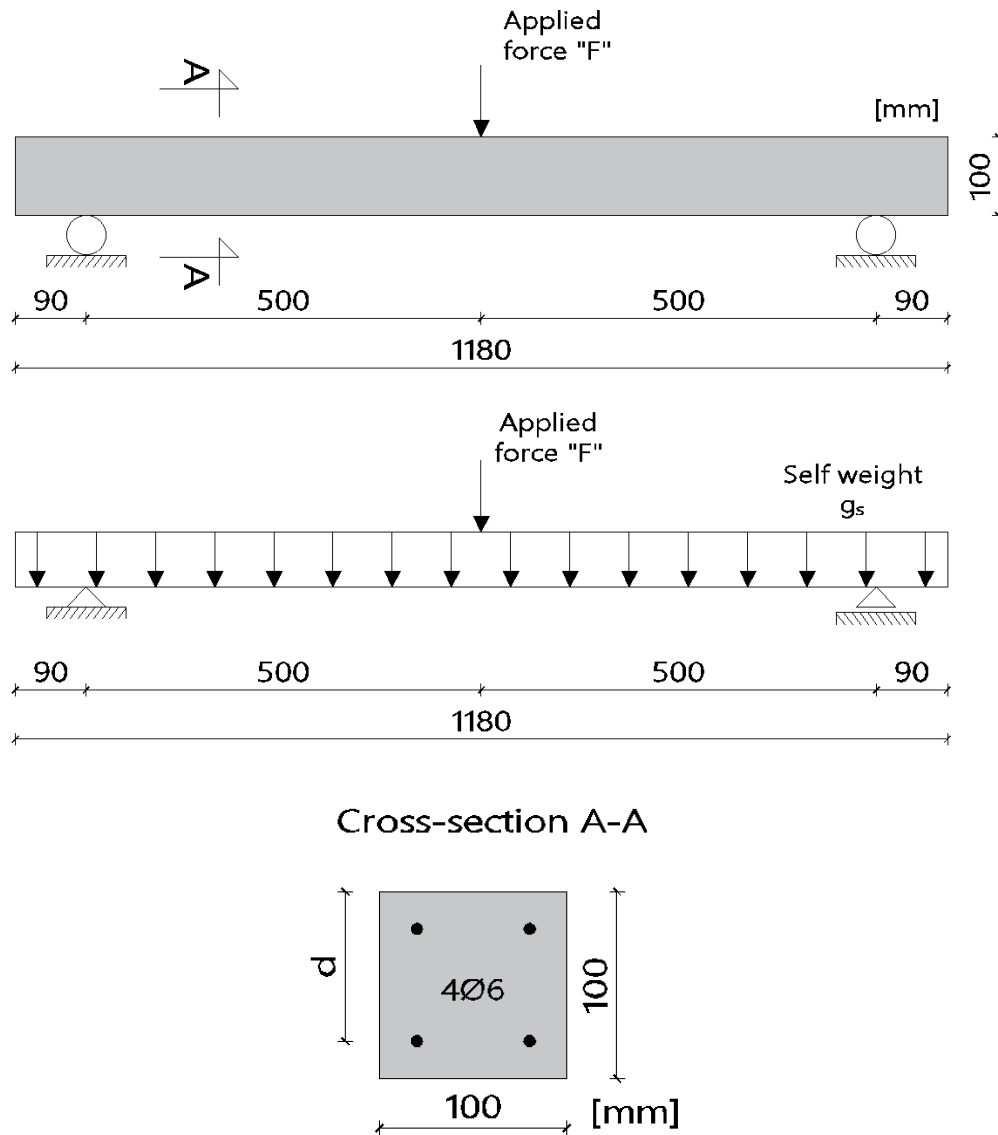
- ACI Committee 224. (2008). Control of Cracking in Concrete Structures- ACI 224R-01. *ACI Manual of Concrete Practice, Part 1*, ACI224R-1-ACI224R-46.
- Balazs, G. L. (1993). Cracking analysis based on slip and bond stresses. *ACI Materials Journal*, 90(4), 340–348.
- Bazant, Z. P., & Oh, B. H. (1983). No Crack band theory for fracture of concrete. *RILEM Publication SARL*, 93(16), 155–177.
- Cai, Q. (2007). Finite element modelling of cracking in concrete gravity dams.
- Chen, W.-F. (2007). . Plasticity in Reinforced Concrete. J. Ross Publishing.
- EN 1992-1-1, 2004. (2004). Eurocode 2: Design of concrete structures – Part 1-1: General rules and rules for buildings. Brussels: CEN European Committee for Standardization. *Journal of Constructional Steel Research*.
- Engström, B. (2011). Design and analysis of continuous beams and columns, 132.
- Johansson, M. (2000). *Structural Behaviour in Concrete Frame Corners of Civil Defence Shelters. Non-linear Finite Element Analyses and Experiment*.
- Jönsson, J., & Stenseke, A. (2018). Concrete Beams Subjected to Drop-Weight Impact and Static Load, 333.
- Knauff, M. (2013). Obliczanie konstrukcji żelbetowych według Eurokodu 2.
- Kobiak, J., & Stachurski, W. (1984). Konstrukcje żelbetowe T.1.
- Kwan, A. K. H., & Ma, F. J. (2016). Crack width analysis of reinforced concrete under direct tension by finite element method and crack queuing algorithm. *Engineering Structures*, 126, 618–627.
- Löfgren et al., I. (2004). Application of WST-method for fracture testing of fibre-reinforced concrete, Chalmers University of Technology, Department of Structural Engineering and Mechanics, Report 04:13, (0170).
- Lozano & Makdesi. (2017). Concrete Beams Subjected to Drop-Weight Impact and Static Load Structural Behavior and Plastic Rotational Capacity from Experiments and Finite Element Analysis.
- Oh, B. H., & Kim, S. H. (2007). Advanced Crack Width Analysis of Reinforced Concrete Beams under Repeated Loads. *Journal of Structural Engineering*, 133(3), 411–420.
- Pędziwiatr, J. (2010). *Wstęp do projektowania konstrukcji żelbetowych wg PN-EN 1992-1-1:2008*.
- Plos et al., M. (2016). A multi-level structural assessment strategy for analysis of RC bridge deck slabs. *19th IABSE Congress Stockholm*, 1559–1566.
- Plos et al., M. (2017). A multi-level structural assessment strategy for reinforced concrete bridge deck slabs. *Structure and Infrastructure Engineering*, 13(2), 223–241.
- Plos, M. (2000). Finite Element Analyses of Reinforced Concrete Structures.
- Rots, J. G. (1988). Computational modeling of concrete fracture, 763, 5–18.
- Tammo et al., K. (2009). Nonlinear analysis of crack widths in reinforced concrete. *Magazine of Concrete Research*, 61(1), 23–34.
- Tejchman, J., & Bobinski, J. (2014). Continuous and Discontinuous Modelling of Fracture in Concrete Using FEM. *International Journal for Numerical and Analytical Methods in Geomechanics*, 313. <https://doi.org/10.1007/978-3-642-28463-2>

Appendix A Calculations

Load capacity of the beam is calculated for a specific cross-section which is located directly in the middle of the beam.

A.1 Input data

A.1.1 Geometry and static scheme of the beam



$$h = 0.1m$$

Beam height

$$b = 0.1m$$

Beam width

$$L = 1.18m$$

Beam length

$$L_i = 1.00m$$

Beam span

$\emptyset = 6mm$	Reinforcement diameter
$c_c = 17mm$	Concrete cover
$A_{s1} = 2\pi \frac{\emptyset^2}{4} = 56.549mm^2$	Bottom reinforcement area
$A_{s2} = 2\pi \frac{\emptyset^2}{4} = 56.549mm^2$	Top reinforcement area
$d = h - c_c - \frac{\emptyset}{2} = 80mm$	Effective depth of a cross-section
$a_2 = h - d = 20mm$	Top reinforcement center of gravity

A.1.2 Concrete properties

$\gamma_c = 1.0$	Partial factor
$f_{cm} = 42.2MPa$	Mean compressive strength after 36 days
$f_{ctm} = 3.7MPa$	Mean tensile strength after 36 days
$f_{cd} = \frac{f_{cm}}{\gamma_c} = 42.2MPa$	Design compressive strength
$\varepsilon_{cu} = 3.5\%$	Ultimate concrete strain
$\lambda = 1.0$	Modification factor for lightweight concrete
$f_r = 0.62\lambda\sqrt{f'_c} = 4.03MPa$	Modulus of rupture of concrete
$G_f = 132.0 \frac{Nm}{m^2}$	Fracture energy
$E_{cm} = 33.9GPa$	Modulus of elasticity after 36 days
$\gamma = 25 \frac{kN}{m^3}$	Reinforced concrete weight

A.1.3 Reinforcement properties

$\gamma_s = 1.0$	Partial factor
$f_u = 686MPa$	Ultimate tensile stress
$f_y = 575MPa$	Mean yield strength
$f_{yd} = \frac{f_y}{\gamma_s} = 575MPa$	Design yield strength

$$E_s = 196 \text{ GPa}$$

Youngs Modulus

$$\varepsilon_{su} = 10.8\%$$

Ultimate steel strain

$$\varepsilon_{sy} = \frac{f_y}{E_s} = 0.293\%$$

Yield strain

A.2 Load capacity excluding top reinforcement

Calculation of load capacity at yield stress:

$$A_s f_{yd} - \xi_{eff} b d f_{cd} = 0$$

Relative compressive height:

$$\xi_{eff} = \frac{A_s f_y}{b d f_{cm}} = 0.096$$

Limit relative compressive height:

$$\xi_{eff,lim} = 0.8 \frac{0.0035}{0.0035 + \frac{f_y}{E_s}} = 0.435$$

$$\xi_{eff} \leq \xi_{eff,lim}$$

Load capacity of the beam at yield stress:

$$M_{u,1} = \xi_{eff} b d^2 f_{cm} (1 - 0.5 \xi_{eff}) = 2.48 \text{ kNm}$$

$$Q_{u,1} = \frac{4 M_{u,1}}{L} = 9.92 \text{ kN}$$

Calculation of load capacity at ultimate stress:

$$A_s f_u - \xi_{eff} b d f_{cm} = 0$$

Relative compressive height:

$$\xi_{eff} = \frac{A_s f_u}{b d f_{cm}} = 0.115$$

Limit relative compressive height:

$$\xi_{eff,lim} = 0.8 \frac{0.0035}{0.0035 + \frac{f_y}{E_s}} = 0.435$$

$$\xi_{eff} \leq \xi_{eff,lim}$$

Load capacity of the beam at ultimate stress:

$$M_{u,2} = \xi_{eff} b d^2 f_{cd} (1 - 0.5 \xi_{eff}) = 2.92 \text{ kNm}$$

$$Q_{u,2} = \frac{4 M_{u,2}}{L} = 11.68 \text{ kN}$$

A.3 Load capacity including top reinforcement

Calculation of load capacity using yield stress:

$$A_{s1}f_y = \xi_{eff} b d f_{cm} + A_{s2}f_y$$

$$\xi_{eff} = \frac{(A_{s1} - A_{s2})}{b d} = 0$$

$$\xi_{eff,lim} = 0.8 \frac{0.0035}{0.0035 + \frac{f_y}{E_s}} = 0.435$$

$$\frac{2a_2}{d} = 0.5$$

$$\xi_{eff} \leq \frac{2a_2}{d}$$

$$M_{u,11} = A_{s1}f_y(d - a_2) = 1.95kNm$$

But not less than:

$$M_{u,1} = 2.48kNm$$

$$Q_{u,1} = \frac{4M_{u,1}}{L} = 9.92kN$$

Calculation of load capacity at ultimate stress:

$$A_{s1}f_t = \xi_{eff} b d f_{cm} + A_{s2}f_t$$

$$\xi_{eff} = \frac{(A_{s1} - A_{s2})}{b d} = 0$$

$$\xi_{eff,lim} = 0.8 \frac{0.0035}{0.0035 + \frac{f_y}{E_s}} = 0.435$$

$$\frac{2a_2}{d} = 0.5$$

$$\xi_{eff} \leq \frac{2a_2}{d}$$

$$M_{u,22} = A_{s1}f_t(d - a_2) = 2.33kNm$$

But not less than:

$$M_{u,2} = 2.93kNm$$

$$Q_{u,2} = \frac{4M_{u,2}}{L} = 11.68kN$$

A.4 Load capacity summary

Load capacity at yield stress:

$$M_{u,1} = 2.48kNm$$

$$Q_{u,1} = 9.92kN$$

Load capacity at ultimate stress:

$$M_{u,2} = 2.93kNm$$

$$Q_{u,2} = 11.68kN$$

A.5 Crack widths calculations

All the calculations are performed for one increment and later on in a similar manner recalculated in a spreadsheet using Microsoft Excel 2018 for all the other cases.

A.5.1 Loads

$i = 120$	Increment number
$F_i = 11.20kN$	Force
$\gamma = 25 \frac{kN}{m^2}$	Reinforced concrete weight
$g_c = \gamma hb = 0.25 \frac{kN}{m}$	Reinforced concrete beam self-weight

A.5.2 Crack widths according to Eurocode 2

Geometric properties in stage I:

$$\alpha_e = \frac{E_s}{E_{cm}} = 5.782$$

$$x_I = \frac{\alpha_e(A_{s2}a_2 + A_{s1}d) + 0.5bh^2}{\alpha_e(A_{s2} + A_{s1}) + bh} = 50mm$$

$$I_I = \frac{bx_I^3}{3} + \frac{b(h - x_I)^3}{3} + \alpha_e[A_{s2}(x_I - a_2)^2 + A_{s1}(d - x_I)^2] = 892.18cm^4$$

$$\sigma_{sI} = \alpha_e \frac{M}{I_I} (d - x_I) = 55.0MPa$$

$$W_c = \frac{I_I}{h - x_I} = 178.44cm^3$$

Maximum moment and cracking moment:

$$M = \left(\frac{g_c L + F_i}{2} \right) \frac{L_i}{2} - g_c \frac{L^2}{8} = 2.83kNm$$

$$M_{cr} = f_{ctm} \cdot W_c = 0.66kNm$$

Geometric properties in stage II:

$$x_{II} = \frac{\alpha_e}{b} \left[-(A_{s1} + A_{s2}) + \sqrt{(A_{s1} + A_{s2})^2 + \frac{2b}{\alpha_e} (A_{s1}d + A_{s2}a_2)} \right] = 19.9mm$$

$$I_{II} = \frac{bx_{II}^3}{3} + \alpha_e[A_{s2}(x_{II} - a_2)^2 + A_{s1}(d - x_{II})^2] = 1.444 * 10^{-6}m^4$$

$$\sigma_{sII} = \alpha_e \frac{M}{I_{II}} (d - x_{II}) = 681.7MPa$$

$$h_{c,eff} = \min \left\{ \begin{array}{l} 2.5(h - d) \\ \frac{(h - x)}{3} \\ h/2 \end{array} \right\} = 26.7mm$$

$$A_{c,eff} = h_{c,eff}b = 2671mm^2$$

$$\rho_{p,eff} = \frac{A_s}{A_{c,eff}} = 0.021$$

$$k_1 = 0.8$$

$$k_2 = 0.5$$

$$k_3 = 3.4$$

$$k_4 = 0.425$$

$$k_t = 0.4$$

Maximum and mean value of crack spacing:

$$s_{r,max} = k_3 c + \frac{k_1 k_2 k_4 \phi}{\rho_{p,eff}} = 106.0mm$$

$$s_{r,m} = \frac{s_{r,max}}{1.7} = 62.4mm$$

$$\varepsilon_{sm} - \varepsilon_{cm} = \frac{\sigma_s - k_t \frac{f_{ct,eff}}{\rho_{p,eff}} (1 + \alpha_e \rho_{p,eff})}{E_s} = 0.003078$$

But not less than:

$$\varepsilon_{sm} - \varepsilon_{cm} = 0.6 \frac{\sigma_s}{E_s} = 0.002087$$

Characteristic and mean value of crack widths:

$$w_k = s_{r,max} (\varepsilon_{sm} - \varepsilon_{cm}) = 0.326mm$$

$$w_m = s_{r,m} (\varepsilon_{sm} - \varepsilon_{cm}) = 0.192mm$$

A.5.3 Crack widths according to ACI 224R

Bar spacing:

$$s = 8cm$$

Geometric properties:

$$\alpha_e = \frac{E_s}{E_{cm}} = 5.782$$

$$I_g = \frac{bh^3}{12} = 8.33 * 10^{-6} m^4$$

$$y_t = \frac{h}{2} = 50mm$$

Maximum moment:

$$M = \left(\frac{g_c L + F_i}{2} \right) \frac{L_i}{2} - g_c \frac{L^2}{8} = 2.83 kNm$$

Calculation of tensile stress in reinforcement at service loads:

$$B = \frac{b}{\alpha_e A_{s1}} = 0.306 mm^{-1}$$

Neutral axis depth:

$$c = \frac{\sqrt{2Bd + 1} - 1}{B} = 19.83mm$$

$$I_{cr} = \frac{bc^3}{3} + \alpha_e A_{s1}(d - c)^2 = 1.444 * 10^{-6} m^4$$

Steel stress:

$$\sigma_s = \frac{M}{I_{cr}} \alpha_e (d - c) = 681.92 MPa$$

Concrete stress:

$$\sigma_c = \frac{M_{srv}}{I_{cr}} c = 38.88 MPa$$

Ratio of distances:

$$\beta = \frac{h - c}{d - c} = 1.333$$

Maximum and mean crack widths:

$$w = 2 \frac{f_s}{E_s} \beta \sqrt{d^2 + \left(\frac{s}{2}\right)^2} = 0.414 mm$$

$$w_m = \frac{w}{1.7} = 0.244 mm$$

A.5.4 Crack widths summary

Characteristic values of crack widths:

$$w_k = 0.326 mm$$

$$w = 0.414 mm$$

According to Eurocode 2

According to ACI 224R

Mean values of crack widths:

$$w_m = 0.192 mm$$

$$w_m = 0.244 mm$$

According to Eurocode 2

According to ACI 224R